Article

ClpP-Deletion Causes Azoospermia, with Meiosis-I Delay and Insufficient Biosynthesis of Spermatid Factors, Due to Mitochondrial Dysfunction with Accumulation of Perrault Proteins ERAL1, PEO1, and HARS2

Suzana Gispert [1#], Jana Key [1#], Aneesha Kohli [1,2], Sylvia Torres-Odio [5], Gabriele Koepf [1], Shady Amr [2], Marina Reichlmeir [1], Patrick N. Harter [6], A. Phillip West [5], Christian Münch [2,3,4] and Georg Auburger [1,*]

1 Exp. Neurology, Medical Faculty, Goethe University, 60590 Frankfurt am Main, Germany; gispert-sanchez@em.uni-frankfurt.de; Jana.Key@kgu.de; Gabriele.Koepf@kgu.de; Marina.Reichlmeir@kgu.de;
2 Institute of Biochemistry II, Goethe University Medical School, 60590, Frankfurt am Main, Germany; aneeshak19@gmail.com; Ch.Muench@em.uni-frankfurt.de; amr@med.uni-frankfurt.de;
3 Frankfurt Cancer Institute, Frankfurt am Main, Germany.
4 Cardio-Pulmonary Institute, Frankfurt am Main, Germany.
5 Department of Microbial Pathogenesis and Immunology, College of Medicine, Health Science Center, Texas A&M University, Bryan, TX 77807, USA; torres.odio@exchange.tamu.edu (S.T.-O.); awest@tamu.edu;
6 Institute of Neurology (Edinger-Institute), University Hospital Frankfurt, Goethe University, Heinrich-Hoffmann-Strasse 7, 60528 Frankfurt am Main, Germany; Patrick.Harter@kgu.de.
Joint first authorship
* Correspondence: auburger@em.uni-frankfurt.de; Tel.: +49-69-6301-7428

Abstract: Human Perrault syndrome (PRLTS) is defined by autosomal recessive inheritance with primary ovarian insufficiency and early hearing loss. Most PRLTS disease proteins modulate mitochondrial transcription or translation. Among the genetic causes are ClpP mutations, which trigger also complete azoospermia, whose cellular and molecular underpinnings are unknown. Here, the ClpP-null mouse model was studied by global transcriptomics, proteomics, RT-qPCR, immunoblots, tissue fractionation, testis histology, and was crossed with STING/IFNAR mutants. Spermatogenesis showed accumulated early spermatocytes, versus deficits of desynapsis and kinetochore factors; excess *Dazl*/*Stra8* and acetylSMC3, versus deficient SHCBP1L, were molecular correlates. Spermiogenesis showed few round spermatids, tsHMG/TFAM in elongated spermatids was absent; transcripts for tail/acrosome factors were downregulated from start. Nuclear anomalies included a failed *Rec8* induction, early BRDT deficiency, histone H3 cleavage, and cGAMP increase, among antiviral responses typical of ClpP-mutants. However, deletion of downstream innate immune signals STING/IFNAR failed to reestablish fertility. As mitochondrial triggers, we observed accumulation of ClpX, with PTCD1, POLDIP2, GRSF1, ALKBH7, DNAJA3, AURKAIP1, VWA8, and Perrault proteins ERAL1, PEO1, HARS2, partially showing nuclear redistribution. ClpP-depletion is known to cause extra-mitochondrial release of mispacked mtDNA/mtRNA/protein complexes. Now we define nuclear inflammatory responses and meiotic arrest as consequences, similar to observations in mito-mice and mutator-mice.

Keywords: meiosis-I; zygotene-pachytene; homologous recombination; H3K9ac; acetyl-tubulin; Twinkle helicase; RMND1; tRNA /rRNA processing; cGAS-STING signaling.

1. Introduction

Azoospermia (the complete absence of sperm from the ejaculate, which leads to complete infertility) was observed so far in one of the rare male individuals with a biallelic missense mutation of the mitochondrial matrix peptidase ClpP, and in all mice with genetic depletion of ClpP [1-3]. Its occurrence in ClpP mutants represents an enigma because

 doi:10.20944/preprints202204.0245.v1

most previously known mitochondrial pathologies have much less impact on testis. Mitochondrial dysfunction usually reduces sperm capacity and fertility only to a degree known as asthenozoospermia [4]. In addition, ClpP mutations result in primary ovarian insufficiency and early-onset hearing loss, a feature combination known as autosomal recessive Perrault syndrome (PRLTS). Thus, ClpP depletion blocks germline differentiation completely, but there is very little knowledge about the molecular events that underlie this clinical condition [5-7]. Across the body of ClpP-null mice cell mitosis occurs normally, although showing a potential delay given their marked growth deficit [8], whereas meiosis appears to be blocked selectively and completely. PRLTS can also be caused by mutations in other factors with functions at the mitochondrial nucleoid, tRNA /rRNA processing, and the mRNA translation apparatus, such as PEO1 (Twinkle), RMND1 (Required for Meiotic Nuclear Division 1 Homolog), PRORP, HARS2, LARS2, and ERAL1 [9-11].

How could such a putative interference with homologous recombination (HR) in the nucleus be caused by a polypeptide cleavage block in mitochondria? ClpP assembles into two heptameric rings, which interact on either side with hexameric rings of the AAA+ ATPase CLPX as substrate-selecting disaggregase, forming a barrel-like structure. The chymotrypsin-like peptide-cleaving activity of ClpP is enhanced by ClpX to a degree where entire proteins can be degraded [12, 13]. Upon ClpP depletion, an excessive accumulation of ClpX protein ensues [1]. There is also a co-accumulation with interactor proteins such as GRSF1, POLDIP2, LRPPRC, GFM1, and other factors known for their action at mitochondrial nucleoids and RNA granules [14]. These are the most consistent consequences across different tissues in mice and humans, and they are accompanied by an enlargement of the nucleoid area and an increased dosage of mitochondrial DNA (mtDNA) [14]. It is important to note that at least in mouse embryonic fibroblasts (MEF), the excess ClpX/GRSF1/GFM1, as well as DNAJA3/STAT1 proteins redistribute to the cell nucleus, with parallel activation of widespread innate immune defenses against toxic DNA/RNA mediated by nuclear cGAS, diffusible cGAMP, and cytosolic STING [14-17]. Retrograde signaling of mitochondrial problems has long been known to trigger nuclear transcriptional responses [18, 19] and might also perturb chromosomal replication and recombination.

With meiosis-I in ovaries occurring before birth, and postnatal maturation of oocytes occurring only for a few cells in each menstrual cycle, it is quite demanding to define the molecular obstacles that cause primary ovarian insufficiency. Therefore, we focused on spermatogenesis which produces about 12 million sperm cells in synchronized stages from mouse postnatal days 10 until 35 (P10-P35) [20], thus revealing upon microscopy where the process is delayed and where it is so disrupted that it triggers complete cell loss. In later mouse life, spermatogenesis asynchronizes, and in advanced adult ages, a testicular inflammation and atrophy of ClpP-null testes hamper analyses [1, 21]. Therefore, three age points were selected for the proteome profiling of dysregulated molecules and enriched pathways in pathogenesis: P17 when meiosis-I should just be completing in early spermatocytes, P21 when meiosis-II should just be finished in late spermatocytes, and P27 when round spermatids should be polarized and acrosome/tail formation should be ongoing. Candidate mitochondrial ClpP-degradation substrate proteins with significant excess abundance were assessed for their relocalization to the nucleus, and immunoblots with RT-qPCR were done for validation and nuclear expression analysis.

When the ClpP-null mouse was characterized in the past [1], WT and mutant testes were subjected to hematoxylin & eosin, electron microscopy, and fluorescent immunohistochemistry for specific markers to define at what differentiation step the production of sperm is delayed or interrupted. The cross-sections of seminiferous tubules revealed normal morphology and numbers for blood vessels, interstitial tissue, Leydig cells, Sertoli cells, and spermatogonia, contrasting with an accumulation of primary spermatocytes in zygotene-pachytene, a very low number of round spermatids, and complete absence of

 doi:10.20944/preprints202204.0245.v1

elongated spermatids & spermatozoa, leading to empty tubular lumina. The ultrastructural analysis of testes revealed that immature acrosomes formed, but tails were completely absent, while mitochondria appeared quite normal.

These microscopic findings are compatible with the notion that mitochondrial pathology slows meiosis-I, but some cells manage to mature until the round spermatid stage. Complete differentiation block and cell death occur when cells should polarize, forming acrosomes, mitochondria-containing midpieces, and tails during spermiogenesis.

Now, the re-analysis of global transcriptomics and the performance of global proteomics permitted to correlate these differentiation hurdles during spermatogenesis to their underlying pathway disruptions and molecular deficiencies, which relate to gain-of-function events for specific mitochondrial proteins. As prime example, absent ClpP-mediated degradation leads to pathological accumulation of at least three other PRLTS disease proteins (namely ERAL1, PEO1/TWNK, HARS2) in mitochondria together with mtDNA/mtRNA, with HARS2 accumulating also in the nucleus. All available evidence suggests that these mitochondrial anomalies then trigger antiviral responses and interfere with nuclear HR after sister chromatid synapsis.

2. Materials and Methods

2.1 Mice and mouse embryonic fibroblasts

The generation of the ClpP-null mice was described in detail before [1], and pups were bred from heterozygous matings. Mice were housed under specific-pathogen-free conditions under a 12 h light cycle with food and water *ad libitum* in the central animal facility (ZFE) of the University Hospital Frankfurt. All animal experiments were performed in compliance with the German animal welfare law. Due to the complete infertility of ClpP-null homozygous mice of both sexes, breeding was done simultaneously among multiple pairs of heterozygous mutation carriers, to then select male homozygous wildtype (WT) and knockout (KO) offspring of matched birth date, aging them under identical conditions until sacrificed for analysis. ClpP-null mice were crossed with STING- and IFNAR- deleted mice as previously described [15].

Mouse embryonic fibroblasts (MEF) were generated as previously reported [1] and cultivated in Dulbecco's minimal essential medium (DMEM) 4.5 g/l glucose (Thermo Fisher Scientific, Waltham, MA, USA, #21969) supplemented with 15% fetal bovine growth serum (Gibco, Thermo Fisher Scientific), 1% Penicillin/Streptomycin (Gibco), and 1% Glutamine (Invitrogen, Waltham, MA, USA) at 37 °C and 5% CO_2 in a humidified incubator, passaging every 3-4 days.

2.2. Light microscopy and immunofluorescence

Oviduct sections were stained with antibodies against DNALI1 (Boster Biological Technologies, Pleasanton, CA, USA, A07656-1; 1:200. Testis tissues were stained with hematoxylin and eosin (H&E) dyes, to assess the absence of elongated spermatids and spermatozoa.

2.3. Transcriptome re-analysis

Affymetrix GeneChip HT MG-430 PM Array Plates had been previously employed to document the global transcriptome profile of ClpP-null versus WT testis (n=3) at the age of 9-10 months [1]. Transcripts with specific functions during the subsequent spermatogenesis stages were now extracted and ordered manually.

2.4. Global proteome profiles by mass spec and label-free quantification

WT and *ClpP*$^{-/-}$ mice (n=3 per age group) were sacrificed at postnatal days P17, P21, and P27, respectively, and their testes were dissected. Per animal, one testis was used for mass spectrometry analyses; the other one was halved and used for RNA and protein isolation.

Preprints (www.preprints.org) | NOT PEER-REVIEWED | Posted: 27 April 2022 doi:10.20944/preprints202204.0245.v1

2.4.1. Sample preparation for Liquid chromatography mass spectrometry (LC-MS)

Testes from WT and ClpP-null mice collected at postnatal days P17, P21 and P27 were washed with ice-cold PBS before being resuspended in hot lysis buffer (2% SDS, 150 mM NaCl, 50 mM Tris–HCl, pH 8, 10 mM TCEP, 40 mM 2-chloracetamide, and protease inhibitor cocktail tablet [EDTA-free, Roche, Basel, Switzerland]) and passed 5 times through a 20 G needle attached to a 1 mL syringe. Lysates were incubated for 10 min at 95 °C, sonicated for 30 s with 1 s ON/1 s OFF pulse at 30% amplitude using Sonics Vibra Cell (Newtown, CT, USA), and incubated for another 10 min at 95 °C.

Sample lysates were prepared as described previously [22]. Briefly, lysates were methanol-chloroform precipitated and the protein pellets were resuspended in 8 M Urea/10 mM EPPS pH 8.2. Protein concentration was determined using the Pierce BCA protein assay kit (Thermo Fisher Scientific). Samples were diluted to 2 M Urea using 10 mM EPPS pH 8.2, and digested overnight with 1:50 (w/w) ratio of LysC (Wako Chemicals, Neuss, Germany) at 37 °C. Samples were further diluted to 1 M Urea and digested with 1:100 (w/w) ratio of sequencing grade Trypsin (Promega, Madison, WI, USA) for additional 6 h at 37 °C. Digests were acidified using trifluoroacetic acid to obtain a pH < 3 and purified using tC18 SepPak columns (50 mg, Waters, Milford, MA, USA). Peptides were dried and resuspended in 0.2 M EPPS pH 8.2, and 10% acetonitrile (ACN). Peptide concentration was determined using Micro BCA protein assay kit (Thermo Fisher Scientific) and 55 µg peptide per sample was labeled with 1:2.5 (w/w) ratio of TMT 10plex labelling reagent (Thermo Fisher Scientific). A bridge channel was prepared by pooling equal amounts from all 18 samples which were TMT-labeled together and split into three sets of equimolar samples for each plex. The samples were organized across three TMT plexes such that one plex contained all three replicates for WT and KO samples for one of the three postnatal days as well as a bridge channel (used only as an additional internal control in this study). The ratios between all channels were further normalized following a single injection measurement of each plex by LC-MS/MS which was also used to control and confirm the labeling efficiency (>99% labeling of all peptide sequences for all plexes). All samples were pooled in equimolar ratios within each plex and acidified before desalting and removal of excess TMT using tC18 SepPak columns (50 mg; Waters). Peptides were dried before fractionation.

2.4.2. High pH reverse phase fractionation

The Dionex Ultimate 3000 analytical HPLC (Thermo Fisher Scientific) was used to perform high pH reverse phase fractionation. For each plex, 385 µg of pooled and purified TMT-labeled samples were resuspended in 10 mM ammonium bicarbonate (ABC), 5% ACN, and separated on a 250 mm long C18 column (X-Bridge, 4.6 mm ID, 3.5-µm particle size; Waters) using a multistep gradient from 100% Solvent A (5% ACN, 10 mM ABC in water) to 60% Solvent B (90% ACN, 10 mM ABC in water) over 70 min. Eluting peptides were collected every 45 s. The resulting 96 fractions were cross-concatenated into 24 fractions and subsequently dried before LC-MS analysis.

2.4.3. LC-MS

5 µg of dried peptides from each fraction were resuspended in 2% (vol/vol) ACN/1% (vol/vol) formic acid (FA) solution and 1 µg was shot. Data acquisition was performed using centroid mode on an Orbitrap Fusion Lumos mass spectrometer hyphenated to an easy-nLC 1200 nano HPLC system with a nanoFlex ion source (Thermo Fisher Scientific). A spray voltage of 2.6 kV was applied with the transfer tube heated to 300 °C and a funnel RF of 30%. Internal mass calibration was enabled (lock mass 445.12003 m/z). Peptides were separated on a self-made, 30 cm long, 75 µm ID fused-silica column, packed in-house with 1.9 µm C18 particles (ReproSil-Pur, Dr. Maisch, Ammerbuch, Germany) and heated to 50 °C using an integrated column oven (Sonation, Biberach, Germany). HPLC solvents consisted of 0.1% FA in water (Buffer A) and 0.1% FA, 80% ACN in water (Buffer B).

Preprints (www.preprints.org) | NOT PEER-REVIEWED | Posted: 27 April 2022 doi:10.20944/preprints202204.0245.v1

Individual peptide fractions were eluted by a nonlinear gradient from 5 to 60% B over 155 min followed by an increase to 95% B in 1 min and held for another 9 min. Full scan MS spectra (350–1,400 m/z) were acquired using the Orbitrap with a resolution of 120,000 at m/z 200, maximum injection time of 100 ms and automatic gain control (AGC) target value of 400,000 at m/z 200. The precursors with a charge state between 2 and 5 per full scan were selected and dependent scans were set to 10. To limit repeated sequencing of already acquired precursors a dynamic exclusion of 45 s and 7 ppm was set and advanced peak determination was deactivated. MS2 precursors were selected with a quadrupole isolation window of 0.7 Th and fragmented by collision-induced dissociation with a normalized collision energy (NCE) of 35% and 10 ms activation time. MS2-analysis was performed in the iron trap with a rapid scan rate using a maximum injection time of 85 ms and an AGC target value of 20,000. Following acquisition of each MS2 spectrum, a synchronous-precursor-selection MS3 scan was collected on the top 10 most intense ions in the MS2 spectrum. MS3 precursors were selected with a quadrupole isolation window of 0.7 Th with multi-notch isolation. Precursors were fragmented by high energy collision-induced dissociation (HCD) with an NCE of 65% and analyzed using the Orbitrap with a resolution of 50,000 at m/z 200 with a scan range of 110-500 m/z, a maximum injection time of 86 ms, an AGC target value of 100,000.

2.4.4. Data analysis

Raw files were analyzed using Proteome Discoverer (PD) 2.4 software (Thermo Fisher Scientific) individually for each plex. Spectra were selected using default settings and database searches were performed using the Sequest HT node in PD against trypsin digested *Mus musculus* reference isoform FASTA (UniProtKB/Swiss-Prot and UniProtKB/TrEMBL; 62,309 sequences; version 10 December 2018) and MaxQuant contaminants FASTA. Static modifications were set as TMT6 (+229.163 Da) at the N-terminus and carbamidomethyl (+57.021 Da) at cysteine residues. Methionine oxidation (+15.995 Da) was set as a dynamic modification. Search was performed using Sequest HT taking the above mentioned modifications into account and additionally with Acetyl (+42.011 Da) modification of the N-Terminus set as dynamic modification. Precursor mass tolerance was set to 7 ppm and fragment mass tolerance was set to 0.5 Da. Default Percolator settings in PD were used to filter peptide-spectrum matches (PSMs). Reporter ion quantifications were achieved using default settings in the consensus workflow. Protein files were exported to Microsoft Excel and the unnormalized abundance values were used for further processing. Sample loading and trimmed mean of M values normalizations were performed consecutively to correct small sample loading and labeling reaction efficiency differences [23]. This was done by multiplying the global scaling factors to each grand total reporter ion intensity of each channel to the average total intensity across the channels using a custom script. The mean $\log_2$ fold-changes were calculated for all quantified proteins in mutant samples with respect to their corresponding WT controls (n = 3 independent biological replicates each). Statistical significance was assessed using a two-sided, unpaired *t* test assuming equal variance using Microsoft Excel 2016. All contaminants were removed before further analysis.

2.5. Reverse transcriptase quantitative PCR

Total RNA from tissues was extracted using TRI reagent according to the manufacturer's protocol (Sigma, Burlington, MA, USA). DNase (Amplification Grade, Invitrogen) was applied, and SuperScriptIII (Invitrogen) was used for reverse transcription following manufacturers' instructions. The qPCRs were performed using TaqMan gene expression assays (Applied Biosystems, Waltham, MA, USA) in cDNA from 20 ng total RNA in 20 µl reactions in a StepOneplus Real-Time PCR system (Applied Biosystems). The following assays were applied: *Adam3*: Mm00456453_m1, *Alkbh7*: Mm01232764_m1, *Aurka*: Mm01248179_g1, *Aurkc*: Mm03039428_g1, *ClpP*: Mm00489940_m1, *Dazl*: Mm012735564_m1, *Dmc1*: Mm00494490_m1, *Dnajb3*: Mm00492548_m1, *Dnajb13*:

 doi:10.20944/preprints202204.0245.v1

Mm00463396_m1, *Dnali1*: Mm00613749_m1, *Eral1*: Mm01742631_s1, *Hars2*: Mm00475675_m1, *Ldhc*: Mm00466648_m1, *Peo1*: Mm00467928_m1, *Poldip2*: Mm00458936_m1, *Prm3*: Mm00443095_s1, *Rec8*: Mm00490939_m1, *Stra8*: Mm00486473_m1, *Sycp3*: Mm00488519_m1, *Tbp*: Mm00446973_m1, *Tex12*: Mm01174533_g1.

2.6. Subcellular fractionation of testis tissues

WT and ClpP$^{-/-}$ (n=3 versus 3) mice were sacrificed at P21 and their testes were dissected. To distinguish different subcellular compartments, cytosolic, mitochondrial, and nuclear fractions were prepared by differential detergent extraction, as previously published [24]. The protein content was determined using BCA assay (Life Technologies, Carlsbad, CA, USA, #23227).

2.7. Quantitative immunoblots

Whole protein extracts from tissues were obtained using RIPA buffer, supplemented with protease inhibitor (cOmplete, Mini Protease Inhibitor Cocktail, Merck Millipore, Darmstadt, Germany, #4693159001) as described before [14]. Protein lysate aliquots of 12.5 µg from either whole protein or subcellular fractions were loaded on SDS gels and quantitative immunoblots were performed as described earlier [1]. Membranes were incubated with the following primary antibodies: acetyl-α-Tubulin (Cell Signaling Technology, Danvers, MA, USA, #9272; 1:1000), acetyl-Histone H3K9 (Cell Signaling, #9649; 1:1000), acetyl-SMC3 (Sigma, MABE1073; 1:1000), cGAS (Cell Signaling, #31659, 1:1000), CLPP (Proteintech, Manchester, UK, 15698-1-AP; 1:1000, CLPX (Invitrogen, PA5-79052; 1:1000), DNAJA3 (Santa Cruz, Dallas, TX, USA, sc-46588; 1:1000), ERAL1 (Proteintech, 11478-1-AP; 1:1000), GRSF1 (Sigma, HPA036985; 1:1000), HARS2 (Proteintech, 11301-1-AP; 1:1000), Histone H3 (Abcam, Cambridge, UK, ab1791; 1:1000), PEO1 (Abcam, ab187517; 1:1000), RMND1 (Abcam, ab223119; 1:1000), TFAM (Merck Millipore, ABE483, 1:1000), Tubulin (Cell Signaling, #2144; 1:1000 or Sigma, #9026, 1:1000). Loading control was done with GAPDH (Calbiochem, Merck Millipore, CB1001; 1:1000) for cytosolic fractions, HSP60 (SantaCruz, sc-13115; 1:500) for mitochondrial fractions, or LAMIN A/C (Abcam, Cambridge, UK, ab169532; 1:1000), for nuclear fractions, and TBP (Abcam, ab63766; 1:500) for whole protein extracts.

2.8. cGAMP ELISA

Approximately, 50 mg of testis (n=9, 5 to 12 months-old male mice) tissue were crushed and lysed in 1% NP-40 lysis buffer, then spun down at 15,000 rpm for 10 min at 4 °C. The supernatant was collected as protein lysate and quantified with micro-BCA assay (#23235, Proteintech). Undiluted protein samples were used to measure cGAMP concentrations using a 2′3′-cGAMP ELISA Kit (Cayman Chemicals, Ann Arbor, MI, USA #501700) in accordance with the manufacturer's protocol.

2.9. Statistical analyses

Statistical analyses and heatmap generation were done using Graphpad Prism software versions 8 and 9. Bar graphs show variances as the standard error of the mean (SEM) and p-values from Welch's t-test (T $0.05 < p < 0.1$; * $p < 0.05$; ** $p < 0.01$; *** $p < 0.001$; **** $p < 0.0001$).

3. Results

Given that sperm tail formation was completely absent in previous microscopy [1], we first tested if this blockage is due to a general ciliogenesis problem. This might also explain the progressive hearing loss of ClpP-null mice since inner ear hair cells depend on cilia function. The motile cilia in the oviduct of female ClpP-null mice were therefore studied histologically and with DNAI1 immunohistochemistry, but appeared normal (Figure S1). Having obtained no evidence for a selective ciliopathy by light microscopy, the study

 doi:10.20944/preprints202204.0245.v1

proceeded to employ molecular surveys to assess (1) in which spermatogenesis stage the cell loss occurs, (2) what pathway dysregulations precede the cell loss, and (3) what the earliest stage of anomalies is where putative mitochondrial interferences start.

3.1. Re-assessment of global transcriptome and validation where spermatogenesis is blocked

A previously documented global transcriptome profile in testis from our ClpP-null mice [1] was re-evaluated, and later compared with the global proteome from early testis age for validation (Supplementary Table S3). We had deposited all transcriptome results in a public database at http://www.ncbi.nlm.nih.gov/geo/query/acc.cgi?acc=GSE40207 (last accessed 21. March 2022), and had already studied the upregulations in detail, showing how mitochondrial pathology triggers the innate immune defenses massively [1, 15-17]. These transcript analyses had shown 10- to 30-fold more dysregulations in testis than in brain, heart, and liver, totaling 7985 upregulations and 4266 downregulations with significances. Endeavoring to identify the prominent pathway alterations, a statistical overrepresentation with p-values of 0.000 was observed for factors clustering in the GeneOntology Biological Processes for "primary metabolic process", "oocyte meiosis", and "gamete generation" among the significant upregulations.

In the successive stages of spermatogenesis, the earliest transcript dysregulation events were observed for cells in zygotene-pachytene (Table 1 left, and Tables S1/2). Subsequent testis proteome profiling efforts at postnatal day 21 (P21) confirmed several findings (Table 1 right). Clearly, the effect sizes of upregulation for the DNA Meiotic Recombinase 1 (*Dmc1* transcript, DMC1 protein) and of downregulation for the synaptonemal complex axial element and SMC family member Kleisin-alpha (*Rec8* transcript, REC8 protein) with its stabilizer protein SGOL2 [25] stood out, and a trend towards downregulation of REC8 and SGOL2 was observed by proteomics already at P17. SGOL2 is also noteworthy since its mutation was reported in one patient with Perrault syndrome [26]. A compilation of spermatogenesis factor transcripts shows upregulations for most HR factors and many isoforms of the anaphase-promoting/kinetochore complex (Table S2), while downregulations preferentially affect the desynapsis factors and massively the spermiogenesis factors (Table S3). These data suggest that unusually strong cellular efforts are being made to maximize meiotic HR, while sister chromatid separation is reduced accordingly.

Preprints (www.preprints.org) | NOT PEER-REVIEWED | Posted: 27 April 2022 doi:10.20944/preprints202204.0245.v1

Table 1. Earliest impact of ClpP-absence on testis pathways was observed for meiotic HR factors. Factors among global transcriptome dysregulations were selected below, if they have established roles in spermatogenesis and represent particularly early events, with their fold-changes and p-values ranked by color gradients in heatmaps (red for upregulation, blue for downregulation). For consistent dysregulations in the global transcriptome at age 9-10 months (left side) and global proteome at postnatal day 21 (right side), the name of each factor was highlighted in color. The columns provide the transcript symbol, oligonucleotide ID under analysis, the adjusted p-value after correction for multiple testing, and the M-value (log2 of fold-change, visualized as a gradient of blue or red shading), versus the protein symbol, UniProt database accession number, p-value, and fold change.

Transcriptome				Proteome			
mRNA Symbol	Oligonucleotide ID	Adj. p-Value	KO - WT testis	Protein Name	UniProt Accession #	p-Value	Fold Change
Cdk1	1448314_PM_at	2.3886E-03	0.9535	**CDK1**	P11440	0.011	0.8427
Cpeb1	1417960_PM_at	5.0444E-06	1.8772				
Dmc1	1449819_PM_at	6.7123E-09	1.5442	**DMC1**	Q61880	0.0088	1.89231
Esco1	1424324_PM_at	3.7664E-06	0.948				
Esco2	1428304_PM_at	2.5428E-06	1.5856				
Exo1	1418026_PM_at	7.2594E-10	2.1744				
M1ap	1449358_PM_at	5.5148E-08	-1.872	**M1AP**	Q9Z0E1	0.0363	1.38218
Mnd1	1452606_PM_at	6.9440E-05	0.9228				
				MSH2	P43247	0.0357	1.16621
				MSH3	E9QPY6	0.0267	0.8157
Msh5	1449537_PM_at	4.4687E-03	0.9091				
Msh6	1416915_PM_at	2.4085E-04	0.9857	**MSH6**	P54276	0.0203	1.18242
Ncapd3	1454952_PM_s_at	3.8077E-03	0.6915				
Ncapg2	1417926_PM_at	5.0388E-06	1.2545				
Ncaph	1423920_PM_at	2.5091E-03	0.8051				
Ncaph2	1429477_PM_at	1.9052E-05	1.012	**NCAPH2**	Q8BSP2	0.0729	1.15707
Pcna	1417947_PM_at	4.8585E-03	0.6386				
Pds5a	1441238_PM_at	3.3764E-03	1.2141				
Pds5b	1435242_PM_at	5.0440E-05	1.0204				
Pds5b	1436161_PM_at	3.0687E-06	1.5893				

Plk1	1448191_PM_at	3.3701E-12	-2.537	**PLK1**	Q07832	0.0229	0.68093
Rad21	1416161_PM_at	3.9712E-09	1.4013	**RAD21**	Q61550	0.0319	1.16952
				RAD21L	R4GML2	0.0232	1.28388
Rad50	1422630_PM_at	2.4492E-03	0.7491	**RAD50**	Q5SV02	0.0256	1.14066
Rad51	1418281_PM_at	1.8260E-07	1.5028				
Rbbp8	1427062_PM_at	1.9516E-03	0.9114				
Rec8	1419147_PM_at	3.2550E-09	-3.477	**REC8**	Q8C5S7	0.0132	0.8087
Sgol1	1418919_PM_at	2.2565E-03	0.8776				
Sgol1	1439510_PM_at	2.0374E-04	0.818				
				SGOL2	Q7TSY8	0.0132	0.79186
Smc1a	1417830_PM_at	4.5976E-07	1.4664				
Smc1a	1417831_PM_at	1.2023E-03	0.6813				
				SMC1B	Q920F6	0.0216	1.18242
				SMC3	Q9CW03	0.0247	1.18854
Smc5	1426270_PM_at	1.6201E-06	1.3961				
				SMC6	Q924W5	0.0024	0.6941
				SMCHD1	Q6P5D8	0.0099	1.18512
Stag1	1421939_PM_a_at	2.0151E-06	1.3715	**STAG1**	Q9D3E6	0.0278	1.12916
Stag1	1421940_PM_at	3.7723E-05	1.1064				
Stag1	1431921_PM_a_at	7.0861E-03	0.7124				
Stag1	1434189_PM_at	2.9004E-07	1.2803				
Stag1	1450420_PM_at	1.7747E-04	1.0022				
Stag2	1421849_PM_at	1.7129E-09	1.9144	**STAG2**	O35638	0.0286	1.209
Stag2	1450396_PM_at	9.3548E-03	-0.882				
				STAG3	O70576	0.0191	1.23567
Sun1	1426666_PM_a_at	1.4948E-04	0.9511				
				SYCP1	Q62209	0.0384	1.12493
Sycp2	1444122_PM_at	5.5607E-05	1.112	**SYCP2**	Q9CUU3	0.142	0.93946

 doi:10.20944/preprints202204.0245.v1

Sycp3	1449534_PM_at	1.4999E-06	1.1736				
Tex12	1421183_PM_at	1.0193E-06	1.5482	**TEX12**	Q9CR81	0.0017	0.78535

3.2. Global proteome evidence at which stage the spermatogenesis is blocked

A hypothesis-free systematic analysis of proteome profiles was done next, with the separate investigation of three stages of sperm maturation at ages P17, P21, and P27. One testis per mouse was used for protein extraction and mass-spectrometry (MS) with label-free quantification of individual peptides, while the other organ was destined for RNA extraction to perform RT-qPCR, and for protein extractions to generate immunoblots (see Figure 1a). Overall, almost 10,000 proteins could be quantified in each MS analysis by the tandem mass tag (TMT) approach, and significant dysregulations were encountered for 223 factors at P17, 1198 factors at P21, and 1423 factors at P27 (Figure 1b, Supplementary Table S3).

Preprints (www.preprints.org) | NOT PEER-REVIEWED | Posted: 27 April 2022 doi:10.20944/preprints202204.0245.v1

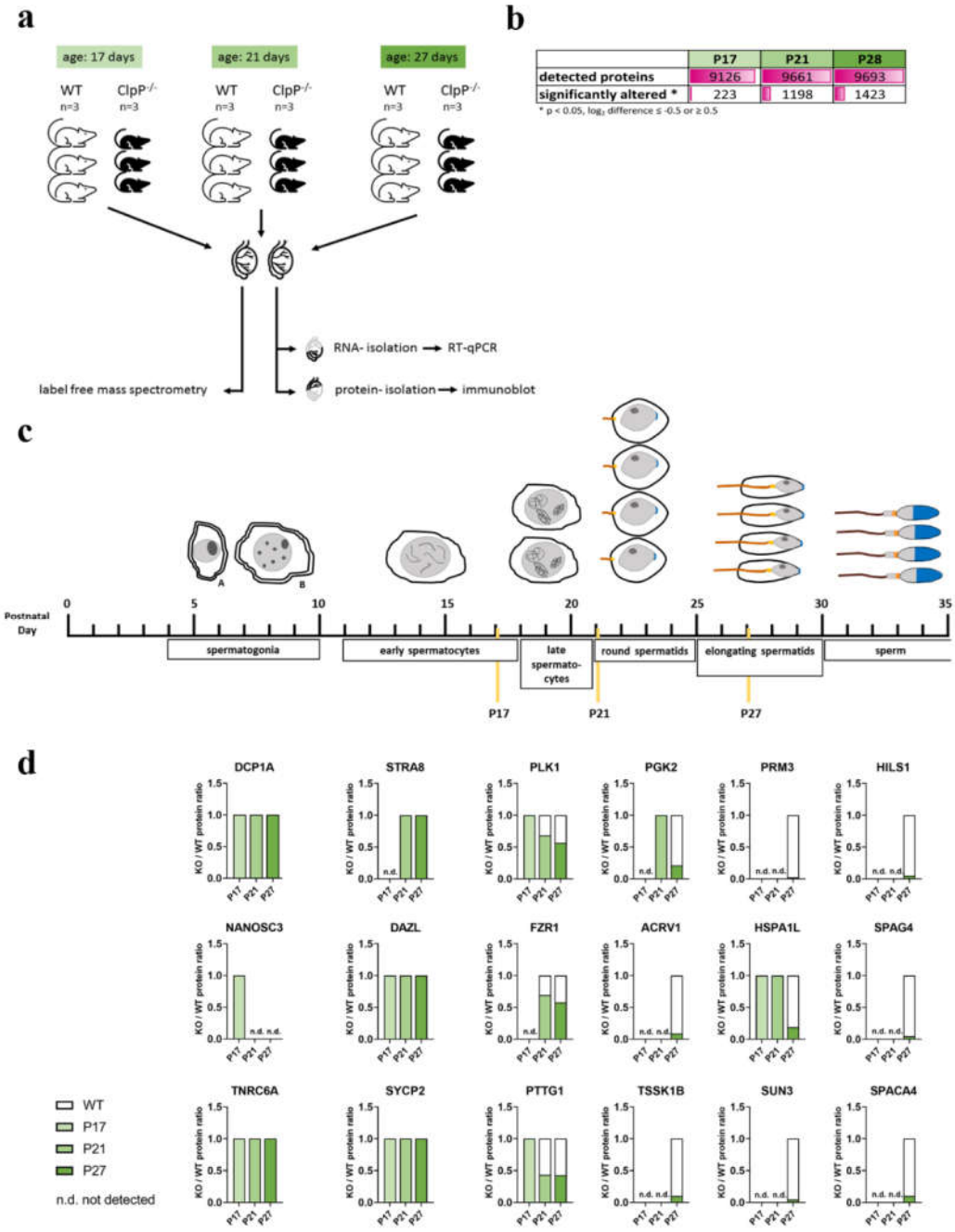

Figure 1. (a) Schematic design of breeding, dissection and extraction of protein and RNA for molecular profiling at three age points. **(b)** Number of successful protein quantifications and of significant dysregulations with relevant effect size (log2 difference ≤-0.5 or ≥0.5) is shown for each age point (shades of green reflect age progression). **(c)** Scheme, illustrating what differentiation stages were studied within the synchronized spermatogenesis during the first 27 postnatal days of mice. **(d)** Mass spectrometry label-free quantification of specific proteins known as markers of successive maturation stages during spermatogenesis. Boxes are normalized to WT, the Y-axis value 1 representing 100%, and a partially green box suggests fewer numbers of cells reaching this stage. A moderate reduction was first observed P21 for late spermatocyte markers PLK1, FZR1, and PTTG1. A massive reduction was observed at P21 for round spermatid markers PGK2, ACRV1, and TSSK1B, while a total loss was observed at P27 for elongating spermatid markers PRM3, and SUN3, as well as for sperm markers HILS1 and SPAG4. n.d. = not detected.

Before the attempt to define selective pathway impairments, it is crucial to control the percentage of cells reaching individual stages of spermatogenesis, and to interpret any molecular dysregulation relative to cell numbers. Established protein markers for each maturation state were compared for ClpP-null versus WT testis at each age point (Figure

 doi:10.20944/preprints202204.0245.v1

1c/d). The markers of spermatogonia DCP1A, NANOSC3, and TNRC6A did not show relevant changes. Early spermatocyte markers STRA8, DAZL, and SYCP2 also had normal protein amounts at all ages. In contrast, late spermatocyte markers PLK1, FZR1, and PTTG1 at P21 and P27 varied between 40% and 70%, suggesting that an impairment and retardation of previous zygotene-pachytene processes decreases the differentiation speed at this stage. Round spermatid markers PGK2, ACRV1 and TSSK1B at P27 showed abundance diminished to 10% or 20%, so only a small minority of cells matures until this stage. Elongating spermatid markers PRM3 and SUN3, as well as sperm markers HILS1, SPAG4, and SPACA4 at P27 showed values around 5%, compatible with the notion of some protein synthesis to occur, but cell maturation to reach a stop.

Overall, the proteome profiles support the cytological observations that early spermatocyte development is delayed and these cells accumulate in pachytene. Thus, fewer cells reach the stage of late spermatocytes where meiosis-II occurs, and only few cells reach the round spermatid stage. Complete interruption and cell elimination are not evident until the process of spermatid polarization during spermiogenesis.

3.3. Proteome and RT-qPCR evidence what prominent pathway alterations lead to block

In an effort to define pathways whose affection precedes and exceeds the cell loss, at each age the significantly dysregulated factors were ranked by fold-change, and prominent effects were compiled in heatmaps, ordered by function (Figure 2a). As known correlates of the mitochondrial impact on asthenozoospermia, early and stable decreases in abundances were observed for bioenergetics proteins COX6B2, COX7B2, LDHC, and LDHAL6B (Figure 2a). The decrease of stress response factor COXFA4L3 (also known as NMES1/MOCCI/C15ORF48) reflects a mitochondrial adaptation within antiviral immunity signaling [27, 28].

As reported [16], this immune activation of ClpP-null cells responds to the release of toxic mtDNA and mtRNA into the cytoplasm, and in testis, the stable accumulations of mtDNA/mtRNA binding mitochondrial proteins such as POLDIP2, PTCD1, GRSF1, ALKBH7 and mitochondrial PRLTS proteins PEO1, ERAL1, HARS2 (Figure 2a) reflected this pathology.

Extra-mitochondrially, similarly strong dysregulations were noted for molecular chaperones and microtubular transport motors, while a more subtle affection concerned components of the meiosis-I machinery. Their consistency or progression is reflected in the heatmap as color gradients (Figure 2a).

Outstanding downregulations already at P17 included the protein kinase CSNK1D (to 15%) that regulates meiosis via REC8 and various microtubular components [29], the CaMKII-dependent GTPase 4930544G11Rik (13%) as microtubule and cell polarity modulating RhoA ortholog [30, 31], the HSPA2 interactor protein SHCBP1L (12%) as meiotic spindle component [32], HSPA2 (34%) as the chaperone mediating chromosomal desynapsis and spindle integrity in male germ cells [33-35], and HSF5 (23%) as the transcription factor responsible for molecular chaperone expression, which is essential for progression through meiotic prophase in spermatogenesis [36]. As a possible consequence, there was a progressively decreased abundance selectively of DNAJ family members (Figure 2a) whose conserved role is in DNA/protein assembly [37].

Strikingly, the motor proteins needed for the spindle pole assembly and for microtubular transport of proteins in the tail (which is devoid of local mRNA translation as all motile cilia [38, 39]) were deficient, with consistency across the three maturation stages and progressively with age. It was curious to note that axonemal dynein assembly factors (DNAAF1/2/3/5, DNALI1, DNAL1/4) show insufficient abundance already at P17 (Figure 2a) long before they are associated with microtubule spokes to structure the tails and to enable retrograde intraflagellar transport [40]. This finding suggests a general biosynthesis deficit. Indeed, a decrease of the gamete-specific acetyl-histone H4 sensor and transcription coordinator BRDT [41] was present already at P17 (0.3-fold) and became significant by P21. BRDT is essential for HR and the completion of meiosis-I. Its deficiency causes

Preprints (www.preprints.org) | NOT PEER-REVIEWED | Posted: 27 April 2022 doi:10.20944/preprints202204.0245.v1

insufficient expression of the post-meiotic transcriptional program in round and elongated spermatid transcription [42-45], so it has become the main pharmacological target molecule to achieve male contraception [46]. Thus, BRDT reduction can explain the impaired biosynthesis of anaphase factors, sperm tail, and acrosome components already evident at P17.

Downregulations of the synaptonemal complex (SC), the cohesin ring, and SC disassembly components became significant by P17 for CENPU and by P21 for PTTG1, ESPL1 (separin), SYCE1L, SMC5/6, PLK1, AURKC, INCENP, CDCA8, BIRC5, MAD2L2, CENPE, PPP2R5C. Relevant upregulations were significant only by P21 for RAD21L, DMC1, STAG1/2/3, and SMC1B/3/4 (Figure 2a).

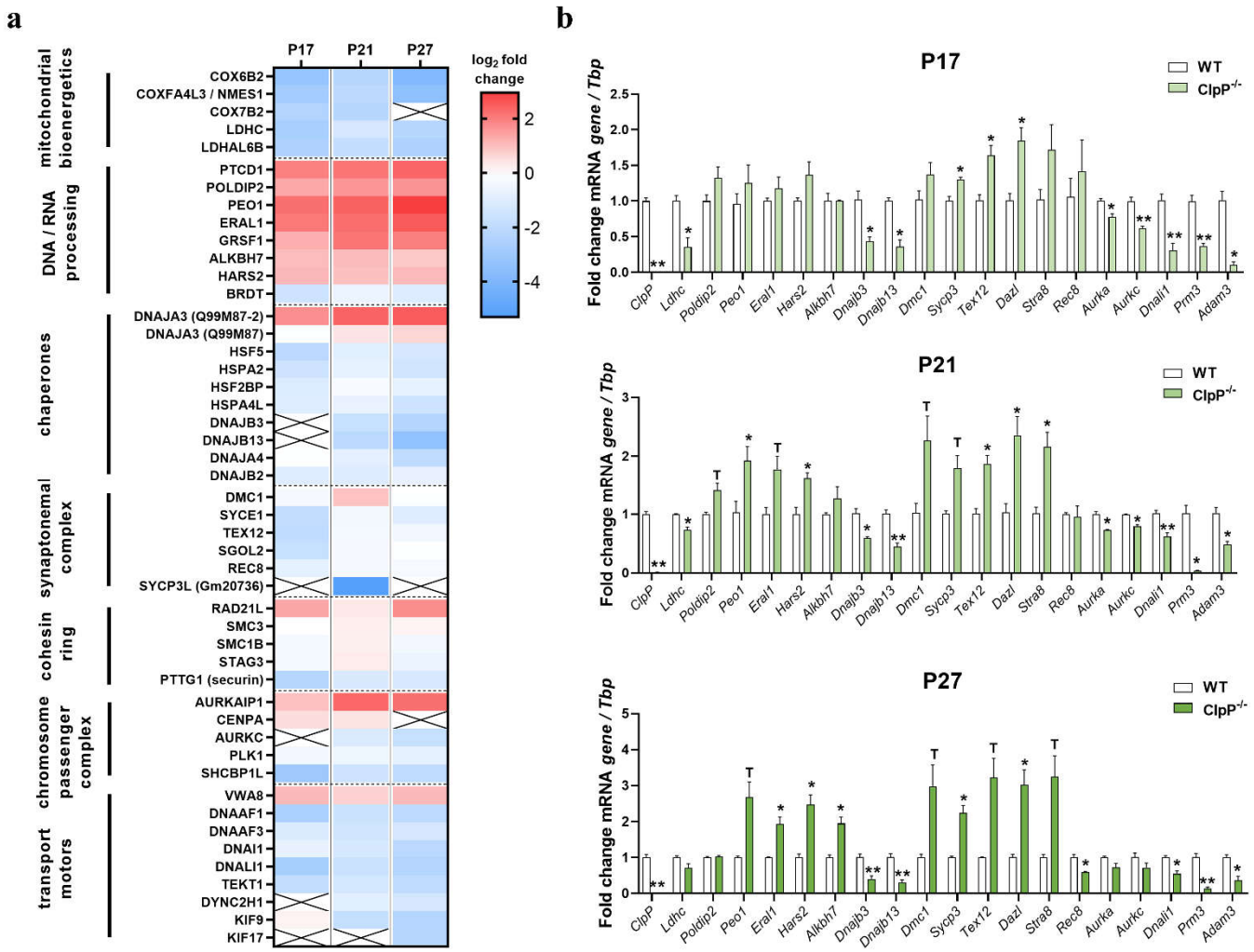

Figure 2. Consistency and progression of proteome and transcript dysregulations during spermatogenesis. (a) Pathways with significant enrichment of dysregulations in the proteome profile of three differentiation stages are selected, with prominent protein components shown as heatmaps with a color gradient illustrating the fold-change (red for upregulation, blue for downregulation). Crossed fields indicate non-detection of that protein. In most cases, the accumulation of mitochondrial pathway members precedes the dysregulation of cytoplasmic pathway members. **(b)** Analysis of transcript levels at the three differentiation stages for key molecules in each pathway usually shows concordant dysregulations to underlie the changed protein abundance, with decreased expression mostly evident already at P17, well before the assembly into differentiated structures takes place. * $p < 0.05$, ** $p < 0.01$, T represents $0.05 < p < 0.10$.

As a main finding of this study into the underlying mitochondrial pathogenesis, the proteome profile revealed ClpP-loss to cause early and consistent accumulation of several PRLTS disease proteins (illustrated by volcano plots in Figure S2), and the RT-qPCR work

Preprints (www.preprints.org) | NOT PEER-REVIEWED | Posted: 27 April 2022 doi:10.20944/preprints202204.0245.v1

showed transcriptional upregulations to underlie this effect. In the heatmap (Figure 2a) among DNA/RNA processing factors, early and consistent accumulation of mitochondrial factors was evident, including PEO1, ERAL1, and HARS2, whose mutations are known to trigger Perrault syndrome with ovarian germ cell failure. While ClpP mutations cause PRLTS3, mutations in the other three PRLTS proteins are responsible for PRLTS5, PRLTS6 and PRLTS2, respectively. PEO1 (also known as TWNK) has a DNA-helicase and a primase domain that preferentially acts at the D-loop of mtDNA [47, 48], so if excess amounts redistribute to the nucleus they might also act at the D-loops that start crossing-over events during meiosis-I. ERAL1 acts as an rRNA chaperone during mitoribosomal biogenesis [49], and its impact on DNA processing is presumably indirect, but it is important to know that mitoribosomal biogenesis is connected with mtDNA replication via parallel expression co-regulation of MRPL43 and PEO1/TWNK by a joint promoter [50, 51]. HARS2 is known as the mitochondrial amino acid synthetase for histidyl-tRNA, which is co-processed with serine-tRNA in a methylation complex involving MRPP3/PRORP, as a further putative Perrault syndrome protein [11, 52-54]. Although ClpP deficiency is thought to impair mitochondrial protein degradation and the excess abundances of PEO1, ERAL1 and HARS2 might be expected to trigger a compensatory expression reduction, on the contrary, a transcript increase appeared already at P17 and became significant at P21/P27. Thus, the induction of these mitochondrial DNA/RNA processing factors seems necessary to compensate for the ClpP loss-of-function.

In agreement with the notion of compensatory efforts to maximize meiosis-I, transcriptional upregulation in RT-qPCR validation experiments was observed for the meiosis inducer *Dazl* (to 235% at P21) and the meiosis inducer *Stra8* (216% at P21) (Figure 2b), as well as several SC/cohesion/HR factors from P17 (*Sycp3*, *Tex12*). Conversely, the cohesin component *Rec8* as well as the desynapsis and polarization factors *Aurka, Aurkc, Dnali1* transcript levels were decreased (Figure 2b). Overall, the RT-qPCR data confirmed the microarray findings in Table S1, and show that meiotic prophase trigger factors *Dazl* and *Stra8*, whose transcription is under the influence of retinoic acid further upstream [55, 56], are activated in response to the maturation block in downstream spermatogenesis. Although the SC axial element component *Rec8* was previously reported to be also induced by retinoic acid [57], a paradoxical transcriptional downregulation of *Rec8* at P27 was observed, and this significant reduction at mRNA and protein level was the first molecular block during ClpP-null spermatogensis observed in the current profiling effort. It is interesting to note that REC8 is regulated by proteolytic cleavage via the downregulated separin, is protected in its centromere association by SGOL2, and is relocalized to associate with mitochondrial surface MAVS during antiviral responses [25, 58, 59]. Thus, REC8 is a key molecule connecting mitochondrial pathology and proteostasis with meiosis.

3.4. Quantitative immunoblot validation of prominent pathway alterations leading to block

To further assess the impaired pathways and to elucidate the involvement of mitochondria, quantitative immunoblots were performed next. The mtDNA-binding transcription factor TFAM in mice has a testis-specific isoform known as tsHMG that localizes only to the nucleus and is produced from the elongated spermatid stage onward [60]. Immunoblots confirmed the complete absence of this nuclear TFAM isoform (Figure 3a). Given that mitochondrially generated acetyl-CoA enables microtubule assembly for spindle dynamics, cell polarization anchored at the two centrioles, and axonemal tail formation, we studied the ratio of acetylated tubulin versus total tubulin (Figure 3b). A massive decrease was observed in 5-month-old testis, probably reflecting the loss of sperm tails due to spermatid apoptosis. This decrease was not observed yet at P17 and P21 (Figure S3a), suggesting that the microtubules of the nuclear spindle apparatus are not affected at this stage, and that anaphase delays cannot be explained by a deficit in acetyl-tubulin. Again, 12-month-old brain tissue showed no acetyl-tubulin change, indicating that sufficient acetyl-CoA is available despite ClpP-dependent mitochondrial dysfunction. In view of the importance of acetylation at K105/K106-SMC3 to stabilize the cohesin

Preprints (www.preprints.org) | NOT PEER-REVIEWED | Posted: 27 April 2022 doi:10.20944/preprints202204.0245.v1

complex and enable chromatid synapsis [61], acSMC3 levels were also evaluated. The immunoblots revealed a >3-fold upregulation in 5-month-old testis (Figure 3c), providing evidence that the acetyl-CoA levels are not restricted by ClpP-dependent mitochondrial dysfunction and that the cells have to make exceptional efforts for HR to occur correctly. Investigation of acSMC3 levels in testis at P17 and P21 were consistent with this finding, although the low sample number precluded significance (Figure S3b). These findings suggest that elevated acSMC3 levels mirror the pachytene delay and that chromatid synapsis alterations are an early feature of azoospermia in our PRLTS3 mouse model.

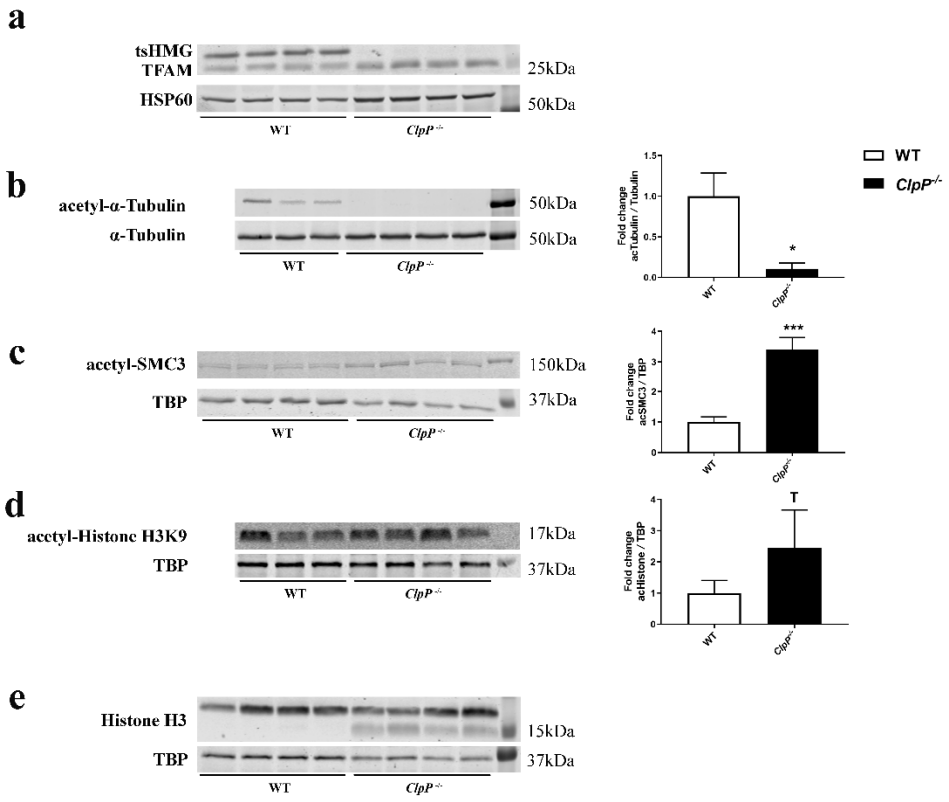

Figure 3. Quantitative immunoblots of whole protein from testis tissues. RIPA-fractions from 5-month-old WT and matched *ClpP*$^{-/-}$ testis were analyzed for **(a)** TFAM with its testis-specific isoform (tsHMG), normalized against mitochondrial HSP60, **(b)** acetyl-α-Tubulin, normalized against α-Tubulin, **(c)** acetyl-SMC3, **(d)** acetyl-histone H3K9, or **(e)** Histone H3. In **(a)** and **(e)**, quantification was not performed, since zero signal would provide unrealistic effect sizes. * $p < 0.05$, *** $p < 0.001$, T represents $0.05 < p < 0.10$.

In view of the strong accumulation of mitochondrial ALKBH7 as a demethylase (see Figure 2a), we next assessed one-carbon metabolism with methylation pathology, which is part of the mitochondrial integrated stress response, particularly upon Twinkle mutation and mitoribosomal translation changes [62-64]. Waves of methylation at different histone lysine positions are a prerequisite for subsequent stages of spermatogenesis [65, 66]. Dysregulation of histone methylation factors in ClpP-null testis proteome at P17 included histone3-lysine9 (H3K9) modulator TRIM33 (0.6-fold) [67] and the H3K4 demethylase activator PCGF6 (0.6-fold) [68], while there was no apparent dysregulation of enzymes for H4-lysine methylation, or H2-lysine acetylation or ubiquitination enzymes. Immunoblots detected only faint smeared bands of H3K9-methyl epitopes without an obvious genotype-dependent difference, but the reciprocal acetylation of H3K9 showed a trend of increase (Figure 3d). H3K9 hypomethylation would preferentially impact meiotic prophase progression [69, 70]. Again, H3K4 methylation immunoblots detected only faint smeared bands of appropriate size in Tricine gels without obvious ClpP-dependent differences.

 doi:10.20944/preprints202204.0245.v1

Serendipitously during these experiments, the immunoblots of total H3 revealed the appearance of a smaller isoform in ClpP-null samples (Figure 3e), of a size known for H3 proteolytic cleavage as cellular stress response, e.g. upon virus infection or DNA damage [71, 72]. Selectively H3 interacts with the chromosomal passenger complex as a phosphorylation target of AURKB [73, 74], so a H3 deficit correlates well with a retardation of anaphase. It is interesting to note that also the H3 sequence homolog CENP-A was reported to undergo cleavage, physiologically during metaphase-anaphase transition [75].

It is conceivable that nuclear anomalies such as failure of *Rec8* transcript induction, cleavage of histone H3, reduced abundance of BRDT, and the mitochondrial deficit of COXFA4L3/NMES1, may constitute events within the antiviral program upon pathological extrusion of mtDNA/mtRNA or the translation stress with colliding mitoribosomes [76] via the cGAS-STING signaling pathway. Therefore the levels of cGAMP were quantified with ELISA technique. cGAMP is an intracellular second messenger synthesized by the nucleotidyltransferase cGAS in response to cytosolic double-stranded DNA that binds STING and stimulates the production of type I interferons [77]. ClpP-null testis showed a significant increase ($p<0.005$; almost 1.5-fold) in cGAMP levels (Figure S4a), consistent with our previous findings of potentiated type I interferon responses and cGAS-STING signaling in various tissues and cells of ClpP-null mice [1, 15]. Given that cGAS is normally kept inactive by tight association with nuclear histones, but can redistribute to the cytosol when toxic DNA appears there or ribosomes collide [76, 78], testis fractionation by differential detergent extraction was used to assess cGAS localization, using GAPDH to control purity of the cytosolic fraction. Unexpectedly, the immunoblot demonstrated exclusively nuclear presence of cGAS also in ClpP-null testis (Figure S4b), compatible with the idea that the pathological mtDNA/mtRNA extrusion exerts its toxicity in the nucleus rather than the cytosol.

However, ablation of STING and type I interferon signaling by genetic deletion of downstream innate immune mediators STING and IFNAR failed to rescue infertility and testis involution, as shown by the lack of mature sperm in the ClpP-null/STING-KO and ClpP-null/IFNAR-KO testis (Figure S4c/d). These results suggest a type I interferon-independent independent role for cGAS activation and cGAMP accumulation in ClpP-null testis. Beyond its role in innate immunity, cGAS has been implicated in several cellular processes, such as genomic instability, DNA damage responses, and cellular senescence [79, 80]. Some of the anomalies in meiosis observed in ClpP-null testis could result from aberrant cGAS activation downstream of mtDNA instability. Future work is required to explore the mechanistic details behind this possibility.

3.5. Redistribution of excess mitochondrial proteins to the nucleus possibly contributes to pathway alterations

Since the nuclear data did not clarify why ClpP deficiency impacts meiosis massively in contrast to mitosis, we next focused on the accumulation of 3 PRLTS proteins in mitochondria of ClpP-null testis, whose mutations also disable germ cell differentiation. In ClpP-mutant fibroblasts, we previously observed that the mitochondrial release of accumulated toxic mtDNA/mtRNA is accompanied by extrusion of their associated proteins such as STAT1 to the cytosol and DNAJA3/GRSF1/GFM1 to the nucleus [14, 16]. To test if also in testis the accumulated mitochondrial DNA/RNA processing proteins get redistributed and may contribute to nuclear pathology, tissue was extracted with differential detergents to obtain the mitochondrial, cytosolic, and nuclear fraction, at P21 when meiosis I should be completed despite delays. Fraction purity was validated with HSP60 as mitochondrial matrix marker, LAMIN-A/C as nuclear membrane markers, and GAPDH as a cytosolic marker, verifying also the complete loss of ClpP from mutant samples ($p=0.0014$) (Figure 4a). ClpX and GRSF1 were detected at the expected sizes (predicted 69 kDa and 53 kDa for the precursor proteins, respectively), their excess abundance in ClpP-null samples was confirmed (mitochondrial CLPX 3.9-fold, $p=0.0192$, mitochondrial GRSF1 6.6-

 doi:10.20944/preprints202204.0245.v1

fold, p=0.0001), and their redistribution to the nuclear fraction was also apparent, although without significance in view of low sample number and high variance (Figure 4b), as previously reported in ClpP-null MEF [14]. Similarly, the accumulation of DNAJA3 in mitochondria led to massive relocalization of its small isoform TID1S (49 kDa as opposed to the full-length protein with 52 kDa) [81] to the nuclear compartment (10-fold, p=0.1524) (Figure 4b), and might therefore be responsible for the repressed expression of the transcription factor HSF5 and its downstream chaperones. PTCD1 accumulation appeared relevant given its impact on 3' end processing of mitochondrial tRNAs and on the repression of mitochondrial leucine tRNA, with its abundance in inverse correlation to COX activity [82, 83]. This pathway is key to the pathomechanism triggered by LARS2 mutations that result in PRLTS. Immunoblot quantification documented PTCD1 abundance to increase significantly (mitochondrial PTCD1 4.0-fold, p=0.0137), without nuclear relocalization.

Commercial antibodies with sufficient sensitivity and specificity to detect dysregulations of endogenous ALKBH7, AURKAIP1 or VWA8 could not be identified.

ERAL1 as an rRNA chaperone is responsible for PRLTS6. In the mitochondrial fraction, immunoblots demonstrated its accumulation (9.8-fold, p=0.0004), while the nuclear fraction of ClpP-null samples showed a subtle accumulation without significance in view of limited statistical power (Figure 4c). PEO1 as the protein responsible for PRLTS5 failed to show the prominent accumulation detected by mass spectrometry (Figure 4c), and exhibited no nuclear localization in testis, despite an immunocytochemical report on its association with the kinetochore of progenitor cells [84], and despite a trend towards nuclear accumulation in ClpP-null MEF (Figure S5). Possible explanations for these discrepancies include the technical differences, with mass spectrometry procedures fragmenting DNA by sonification while the fractionation protocol used DNA digestion by benzoase; immunocytochemical cross-reactivity with kinetochore components is a frequent artifact. Instead, the PEO1 immunoblot suggested altered isoform processing with less TWINKLE (77 kDa, 0.4-fold, p=0.055) but apparently more TWINKY (66 kDa). Twinky was described in humans as unable to associate with the D-loop of mtDNA due to its loss of the C-terminal homo-multimerization domain [85]. PEO1 and HARS2 were the only PRLTS proteins with significant accumulation in mass spectrometry already at P17. HARS2 as the protein responsible for PRLTS2 showed not only significant 1.5-fold mitochondrial accumulation (p=0.0434) but also a completely novel redistribution to the nucleus even in WT samples (Figure 4c). Although the presence of this mitochondrial PRLTS protein in the nucleus might contribute to the meiotic impairment, the mechanism remains unclear since the physiological effects of nuclear HARS2 are currently unknown. RMND1, responsible for PRLTS with renal involvement, was investigated although it did not appear dysregulated in the proteome survey, given that its first description in yeast and its name imply a role in meiosis. It showed accumulation within mitochondria in the immunoblots (2.7-fold, p<0.0001), but no re-localization to the nuclear department.

Preprints (www.preprints.org) | NOT PEER-REVIEWED | Posted: 27 April 2022 doi:10.20944/preprints202204.0245.v1

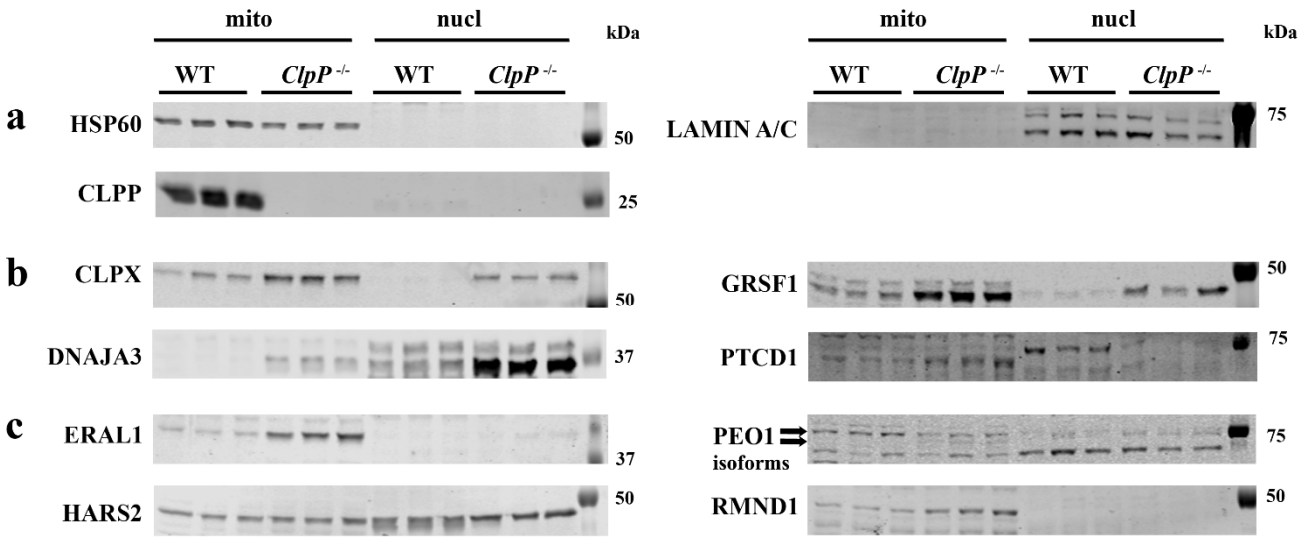

Figure 4. Excess of mitochondrial proteins can trigger redistribution to nuclear fraction. Testis P21 was fractionated with differential detergents and protein extracts were analyzed by quantitative immunoblots, normally blocked with BSA. **(a)** Fractionation purity was controlled by mitochondrial marker HSP60 and nuclear membrane markers LAMIN-A/C, sample genotype was controlled by assessment of ClpP presence. **(b)** Evident relocalization from mitochondria to nuclei was again observed for excess ClpX and its interactome component GRSF1, as well as the mature small isoform TID1S of DNAJA3. In contrast, the accumulation occurred purely in mitochondria for PTCD1. **(c)** Immunoblots confirmed ClpP to modulate the abundance of several PRLTS proteins. ERAL1 was accumulated in the mitochondrial fraction, and a faint band was apparent in mutant nuclear fractions. In contrast, PEO1 detection with a commercial rabbit polyclonal antibody directed against the C-terminal-half showed a decrease of full-length 77 kDa Twinkle band with the parallel accumulation of 66 kDa Twinky band (arrows on the left side). A nuclear redistribution was not detected for any PEO1 isoform. HARS2 immunoreactivity of appropriate molecular weight was observed in the nucleus even for WT samples, with strong accumulation for ClpP-null samples. The assessment of RMND1 also suggested mitochondrial accumulation, but no presence in the nucleus.

4. Discussion

This study of ClpP-null associated azoospermia provided several novel and important insights.

(i) Within its functional pathway inside mitochondria, the loss-of-function of PRLTS3 protein ClpP is compensated transcriptionally by the induction of several other PRLTS proteins, certainly ERAL1, Twinky, HARS2, and possibly RMND1; among them, HARS2 has a physiological localization in the nucleus that is increased in the mutant.

(ii) Within mitochondria overall, ClpP absence is known to have a prominent impact on the inner membrane COX complex activity, the rate-limiting step of respiration, as previously reported [1], and lactate metabolism, while metabolic functions such as acetylation or methylation in this study showed no gross anomaly. COX function should be adjusted to testis-specific needs by the isoforms COX6B2 and COX7B2 and adapted to antiviral stress by the subunit COXFA4L3, but these proteins showed outstanding stable downregulations in testis already at P21. Furthermore, the COX activity repressor PTCD1 exhibited early and strong upregulation, as shown in Figures 2 and 4.

(iii) In agreement with a role of ClpP for proteostasis and unfolded protein responses, the molecular chaperone pathway in mitochondria and also in the cytosol was dysregulated early on and progressively. In this context, it is noteworthy that a UPRmt study in *C. elegans* showed retrograde signaling to the nucleus to activate the ubiquitin homolog UBL5, which is a key factor for sister chromatid cohesion via sororin/CDCA5 that associates with acetyl-SMC3 [62, 86].

 doi:10.20944/preprints202204.0245.v1

(iv) The selective massive affection of spermatogenesis upon microscopy was due to a delay of meiosis-I in pachytene spermatocytes, with subsequent failure to polarize cells at the spermatid stage. This was reflected by an induction of *Dazl*/*Stra8* and most spermatocyte factors until HR, while the subsequent factors of desynapsis and spermiogenesis were generally downregulated at transcript and protein levels. The absence of spermatid tail formation is not due to a generalized ciliogenesis defect, given that we observed normal cilia in the ClpP-null mouse oviduct. Also ClpP-null ovaries seem to experience problems at the stage of meiosis-I, in view of a report that their transcriptional profile at the ages of 6 and 3 months revealed a prominent 7-fold and 9-fold induction, respectively, for *Hormad1* mRNA as a factor needed upon chromatid synapsis failure [7, 87]. Not only in ClpP-null mice the mtDNA pathology impedes HR, but two more examples are known from the literature: Firstly, male infertility with an arrest in meiosis-I and abnormal sister chromatic synapsis was observed in mito-mice that inherit a pathogenic 4,696-bp deletion in mtDNA [88]. Secondly, male infertility due to pachytene spermatocyte loss occurs in mutator mice due to a mutation of the mtDNA Polymerase Gamma (PolG), and it was rescued by TFAM overexpression and increased total mtDNA DNA copy number [89]. Furthermore, is was observed in cell culture experiments that reduced levels of mtDNA and TFAM via retrograde signaling have a prominent downregulation effect on the transcript levels of condensin component *Ncapg2* [90]. In ClpP-null testis where mtDNA is elevated we conversely observed increased *Ncapg2* levels (see Table S1). Jointly, all these observations support the notion that mtDNA dosage specifically interacts with the maturation of pachytene spermatocytes, chromatid synapsis, and HR, by poorly defined mechanisms. It is therefore possible in ClpP-null testis that the complete absence of the mtDNA-binding TFAM isoform tsHMG (which localizes only to the nucleus) reflects this pathogenesis and contributes to it. However, our findings indicate that pathway alterations appear long before the stage when tsHMG immunoreactivity becomes strong in elongated spermatids. Overall, our data suggest that several pathogenesis cascades start from mtDNA/mtRNA and the associated proteins, in parallel in pachytene spermatocytes, as well as in subsequent stages of spermiogenesis, as discussed below.

(v) Nuclear pathology events observed here, such as *Rec8* transcript induction deficits, aberrant histone H3 cleavage, reduced BRDT abundance and the activation of nuclear cGAS, may be interpreted within the general pattern of innate immunity activation against toxic mtDNA/mtRNA that characterizes ClpP-null cells [15, 16]. Although the azoospermia of ClpP-null mice was not mitigated when downstream immune signals were blocked by genetic deletion of STING and IFNAR, it is possible that mtDNA pathology impacts meiosis further upstream in the antiviral program. One example is the sequestration of nuclear REC8 to the mitochondrial outer membrane in association with the MAVS protein upon virus exposure [91], but there are presumably other unknown direct interactions that do not depend on type I interferon production.

(vi) The extrusion of mtDNA/mtRNA from stressed mitochondria can occur in association with their binding proteins, as demonstrated by the nuclear relocalization of accumulated ClpX, GRSF1, DNAJA3, and HARS2. Beyond the generalized upregulation of spermatocyte transcripts and the generalized downregulation of spermatid transcripts, these mtDNA/mtRNA-associated proteins appear to trigger selective dysregulations within their pathways from earliest spermatogenesis stages.

For example, the strongly increased protein abundance of the G-quadruplex (G4) RNA unwinding factor GRSF1 might underlie upregulated *Dazl* transcript levels. GRSF1 is physiologically present both in mitochondria and the nucleus, as other members of the hnRNP F/H family [92]. Its abundance is regulated by DAZL [93] as a spermatogenesis master translational regulator [92, 94]. Excess nuclear GRSF1 might already influence the differentiation from spermatogonia to early spermatocytes since it is known that a G4-repeat DNA structure resolvase named RHAU is essential for this maturation step via c-Kit [95].

 doi:10.20944/preprints202204.0245.v1

For the extra-mitochondrial progressive decreases of molecular chaperones within the DNAJ family since P17, and the downregulation of the chaperone-regulating transcription factor HSF5, again a potential mitochondrial trigger exists: the early accumulation of mitochondrial DNAJA3, which is redistributed to the nucleus where it influences STAT transcription factors [16] and may reduce the levels of HSF5 and its downstream chromatid desynapsis chaperone HSPA2 [33, 34].

The dysregulations among factors of the SC, cohesin ring, SAC, and kinetochore from P21 onwards might be consequences of the prior accumulation (already at P17) of mitochondrial DNA/RNA processing factors such as POLDIP2, PEO1, ALKBH7, and HARS2. POLDIP2 was described as mainly mitochondrial, but stress conditions are known to lead to its nuclear redistribution [14, 96, 97]. Although PEO1/Twinkle-like immunoreactivity was observed at the kinetochore during progenitor cell division [84], and although the PEO1 helicase domain could interfere with nuclear D-loops during HR, we found no evidence for its accumulation in the nucleus with the antibody employed. Given the UniProt evidence that many diverse PEO1 helicase fragments exist as isoforms in different cell types, it is impossible to exclude that specific antibodies fail to detect the nuclear redistribution of PEO1 cleavage products since they may detect unsuitable epitopes. ALKBH7 was recently reported as crucial demethylase for nascent polycistronic mtRNA [98] and its potential nuclear relocalization might impair epigenetic regulations there. The physiological presence of HARS2 and its ClpP-dependent accumulation in the nucleus are completely new, and their role in meiosis-I and HR remains to be studied.

Similarly, the CPC factor dysregulations from P21 might respond to the accumulation from P17 of mitochondrial AURKAIP1, given that this protein was identified as mitoribosomal component (also known as MRPS38), but it was also observed to act as negative regulator of Aurora Kinase A, which localizes at centrosomes and is a key coordinator of anaphase [99-103]. Prominently Aurora Kinases A and C are known as signal regulators that coordinate meiotic desynapsis, spindle assembly, and tail formation [104, 105]. Thus, the transcript reductions observed for both of them (*Aurka* and *Aurkc* in Table 1) may underlie a retardation in anaphase and in ciliogenesis. The transcript reductions observed for *Plk1* would have a similarly delaying effect. A prominent phosphorylation target of Aurora Kinase A is Astrin (gene symbol *Knstrn*) [102-104], whose transcript levels showed exceptional downregulation (Table 1).

5. Conclusions

Overall, we report the first proteome profiles of ClpP-null testis with validation experiments by RT-qPCR, immunoblots, fractionations, ELISA and histology. The complete failure of spermatogenesis is reflected by almost complete meiotic arrest despite transcriptional induction of relevant mediators, followed by deficient biosynthesis of anaphase and spermiogenesis factors. The absence of ClpP in mitochondria appears to disrupt nuclear sister chromatid synapsis and homologous recombination via mechanisms that involve the accumulation of mtDNA/mtRNA with their associated proteins and their extra-mitochondrial release. Several events in nuclear pathology are part of antiviral programs, in keeping with the observation of elevated cGAMP levels in ClpP-null testis, but the elimination of downstream immune signaling does not prevent azoospermia. Importantly, the depletion of ClpP leads to compensatory transcriptional inductions and protein accumulation for three other PRLTS disease proteins, namely ERAL1, PEO1, and HARS2.

Supplementary Materials: Figure S1: Immunohistochemistry of ClpP-null oviduct. **Figure S2**: ClpP-null testis global proteome volcano plots at three ages. **Figure S3**: Quantitative immunoblots to validate proteome profile. **Figure S4**: ELISA quantification of testis homogenate cGAMP levels, immunoblot of cGAS in cytosolic and nuclear testis fractions, and H&E staining of double knockout mice with STING and IFNAR. **Figure S5:** PEO1 isoforms in ClpP-null MEF fractions. **Table S1**: ClpP-null testis transcript upregulations at age 9-10 months, **Table S2**: ClpP-null testis transcript downregulations at age 9-10 months. **Table S3.** Mass-spectrometry data.

Author Contributions: Conceptualization, S.G., A.P.W., C.M. and G.A.; methodology, S.G., J.K., S.T.-O., G.K., S.A., P.N.H. and C.M.; software, A.K. and S.A.; validation, S.G., J.K., G.K., M.R., P.N.H. and G.A.; formal analysis, S.G., J.K., A.K., C.M. and G.A.; investigation, S.G., J.K., G.K. and G.A.; resources, S.G., J.K., S.T.-O., A.P.W. and G.A.; data curation, A.K. and C.M.; writing—original draft preparation, S.G., J.K. and G.A.; writing—review and editing, S.G., J.K., P.N.H., A.P.W., C.M. and G.A.; visualization, S.G., J.K., S.T.-O., P.N.H., A.P.W. and G.A.; supervision, S.G., J.K., A.P.W., C.M. and G.A.; project administration, G.A.; funding acquisition, P.N.H., A.P.W., C.M. and G.A. All authors have read and agreed to the published version of the manuscript.

Funding: This research was supported by internal funds of the Goethe University Medical Faculty in Frankfurt/Main. S.T-O. was supported by predoctoral training award F31HL160141 from the National Heart, Lung, and Blood Institute, National Institutes of Health (NIH). A.P.W. was supported by an Office of the Assistant Secretary of Defense for Health Affairs, U.S. Department of Defense Peer Reviewed Medical Research Program award W81XWH-20-1-0150, and grant R01HL148153 from the National Heart, Lung, and Blood Institute, National Institutes of Health (NIH). C. Münch acknowledges support from the European Research Council under the European Union's Seventh Framework Programme (ERC StG 803565), the Deutsche Forschungsgemeinschaft (DFG, German Research Foundation) Project-ID 390339347 (Emmy Noether Programme) and Project-ID 403765277 (mass spectrometer).

Institutional Review Board Statement: The mouse breeding and dissection study was conducted according to the guidelines of the Declaration of Helsinki, and approved by the Institutional Review Board at the Regierungspräsidium Darmstadt (V54 - 19c 18 - FK/1083 on March 27, 2017).

Data Availability Statement: Testis LC-MS proteomics data have been deposited in the ProteomeXchange Consortium via the PRIDE [106] partner repository with the PXD033388.

Acknowledgments: We are thankful for the help received from the staff at the ZFE Animal Facility of the Medical Faculty of Frankfurt University. We thank G. Tascher and the Quantitative Proteomics Unit (IBC2, Goethe University Frankfurt) for proteomics support. The bioinformatics support by Kevin Klann is gratefully acknowledged.

Conflicts of Interest: The authors declare no conflict of interest. The funders had no role in the design of the study; in the collection, analyses, or interpretation of data; in the writing of the manuscript, or in the decision to publish the results.

Abbreviations:

AAA+	ATPases Associated with diverse cellular Activities
ABC	ammonium bicarbonate
ACN	acetonitrile
ACRV1	Acrosomal Vesicle Protein 1
ACTB	Actin Beta
ADAM3	ADAM Metallopeptidase Domain 3A
AGC	automatic gain control
ALKBH7	AlkB Homolog 7
AURKA	Aurora Kinase A
AURKAIP1	Aurora Kinase A Interacting Protein 1
AURKC	Aurora Kinase C
BCA	Bicinchoninic acid assay
BET	Bromodomain and extraterminal domain
BIRC5	Baculoviral IAP Repeat Containing 5
BRDT	Bromodomain Testis Associated
BSA	Bovine serum albumin
CDCA8	Cell Division Cycle Associated 8
CENPE	Centromere Protein E
CENPU	Centromere Protein U
cGAMP	Cyclic guanosine monophosphate–adenosine monophosphate
cGAS	Cyclic GMP-AMP Synthase
CLPP	Caseinolytic Mitochondrial Matrix Peptidase Proteolytic Subunit
CLPX	Caseinolytic Mitochondrial Matrix Peptidase Chaperone Subunit X
CPC	Chromosome passenger complex

 doi:10.20944/preprints202204.0245.v1

CSNK1D	Casein Kinase 1 Delta
DAZL	Deleted In Azoospermia Like
DCP1A	Decapping MRNA 1A
DMC1	DNA Meiotic Recombinase 1
DNAAF	Dynein Axonemal Assembly Factor 1
DNAJA3	DnaJ Heat Shock Protein Family (Hsp40) Member A3
DNAJB13	DnaJ Heat Shock Protein Family (Hsp40) Member B13
DNAJB3	DnaJ Heat Shock Protein Family (Hsp40) Member B3
DNALI1	Dynein Axonemal Light Intermediate Chain 1
ELISA	Enzyme-linked Immunosorbent Assay
EPPS	*N*-(2-Hydroxyethyl)piperazine-*N*′-(3-propanesulfonic acid)
ERAL1	Era Like 12S Mitochondrial RRNA Chaperone 1
ESPL1	Extra Spindle Pole Bodies Like 1, Separase
FA	formic acid
FZR1	Fizzy And Cell Division Cycle 20 Related 1
GAPDH	Glyceraldehyde-3-Phosphate Dehydrogenase
GFM1	G Elongation Factor Mitochondrial 1
GRSF1	G-Rich RNA Sequence Binding Factor 1
GTP	Guanosine triphosphate
HARS2	Histidyl-TRNA Synthetase 2, Mitochondrial
HCD	high energy collision-induced dissociation
HILS1	H1.9 Linker Histone, Pseudogene
hnRNP	Heterogeneous Nuclear Ribonucleoprotein
HPLC	High performance liquid chromatography
HR	homologous recombination
HSF5	Heat Shock Transcription Factor 5
HSP60	Heat Shock Protein Family D (Hsp60) Member 1
HSPA1L	Heat Shock Protein Family A (Hsp70) Member 1 Like
ID	inner diameter
IFNAR	Interferon (alpha and beta) receptor 1
INCENP	Inner Centromere Protein
kDA	kiloDalton
KO	Knockout
LARS2	Leucyl-TRNA Synthetase 2, Mitochondrial
LC-MS	Liquid chromatography–mass spectrometry
LDHC	Lactate Dehydrogenase C
LRPPRC	Leucine Rich Pentatricopeptide Repeat Containing
MAD2L2	Mitotic Arrest Deficient 2 Like 2
MAVS	Mitochondrial antiviral signalling protein
MS	Mass spectrometry
MEF	Mouse embryonic fibroblasts
mRNA	Messenger RNA
MRPL43	Mitochondrial Ribosomal Protein L43
MS	Mass spectrometry
mtDNA	Mitochondrial DNA
n.d.	Not detected
NANOS3	Nanos C2HC-Type Zinc Finger 3
NCAPG2	Non-SMC Condensin II Complex Subunit G2
NCE	normalized collision energy
NLR	Nod-like receptor
NMES1	Normal mucosa of esophagus-specific gene 1
PBS	Phosphate-buffered saline
PCGF6	Polycomb Group Ring Finger 6
PD	Proteome Discoverer software
PEO1	Progressive external ophthalmoplegia (=Twinkle)

 doi:10.20944/preprints202204.0245.v1

PGK2	Phosphoglycerate Kinase 2
PLK1	Polo Like Kinase 1
POLDIP2	DNA Polymerase Delta Interacting Protein 2
PolG	Polymerase Gamma
PPP2R5C	Protein Phosphatase 2 Regulatory Subunit B'Gamma
PRLTS	Perrault syndrome
PRM3	Protamine 3
PRORP	Protein Only RNase P Catalytic Subunit
PSM	peptide-spectrum matches
PTCD1	Pentatricopeptide Repeat Domain
PTTG1	PTTG1 Regulator Of Sister Chromatid Separation, Securin
RAD21L	RAD21 Cohesin Complex Component Like 1
REC8	REC8 Meiotic Recombination Protein
RF	radio frequency
RHAU	RNA Helicase Associated With AU-Rich Element Protein
RIPA	Radioimmunoprecipitation assay buffer
RMND1	Required For Meiotic Nuclear Division 1 Homolog
RNA	Ribonucleic acid
Rpm	revolutions per minute
RT-qPCR	Reverse transcriptase quantitative polymerase chain reaction
SAC	Spindle assembly checkpoint complex
SC	Synaptonemal complex
SDS	Sodium dodecylsulfate
SEM	Standard error of the mean
SGOL2	Shugoshin 2
SHCBP1L	SHC Binding And Spindle Associated 1 Like
SMC1B	Structural Maintenance Of Chromosomes 1B
SMC3	Structural Maintenance Of Chromosomes 3
SPACA4	Sperm Acrosome Associated 4
SPAG4	Sperm Associated Antigen 4
STAG1/2/3	Stromal Antigen 1/2/3
STAT1	Signal Transducer And Activator Of Transcription 1
STING	Stimulator Of Interferon Response CGAMP Interactor 1
STRA8	Stimulated By Retinoic Acid 8
STRING	Search tool for recurring instances of neighbouring genes
SUN3	Sad1 and UNC84 domain containing 3
SYCE1L	Synaptonemal Complex Central Element Protein 1 Like
SYCP3	Synaptonemal Complex Protein 3
TBP	TATA-Box Binding Protein
TCEP	Tris(2-carboxyethyl)phosphin
TEX12	Testis Expressed 12
TFAM	Transcription Factor A, Mitochondrial
Th	Thomson (mass-to-charge ratio as mass spectrometry unit)
TID1S	Tumorous Imaginal Discs Protein Tid56 Homolog
TLR	Toll-like Receptor
TMT	Tandem mass tag
TNRC6A	Trinucleotide Repeat Containing Adaptor 6A
TRIM33	Tripartite Motif Containing 33
tRNA	transfer RNA
tsHMG/TFAM	testis-specific High-Mobility Group protein (TFAM testis isoform)
TSSK1B	Testis Specific Serine Kinase 1B
VWA8	Von Willebrand Factor A Domain Containing 8
WT	Wildtype
ZFE	Central animal facility

References

1. Gispert, S., et al., *Loss of mitochondrial peptidase Clpp leads to infertility, hearing loss plus growth retardation via accumulation of CLPX, mtDNA and inflammatory factors.* Hum Mol Genet, 2013. **22**(24): p. 4871-87.
2. Jenkinson, E.M., et al., *Perrault syndrome is caused by recessive mutations in CLPP, encoding a mitochondrial ATP-dependent chambered protease.* Am J Hum Genet, 2013. **92**(4): p. 605-13.
3. Demain, L.A., et al., *Expanding the genotypic spectrum of Perrault syndrome.* Clin Genet, 2017. **91**(2): p. 302-312.
4. Vertika, S., K.K. Singh, and S. Rajender, *Mitochondria, spermatogenesis, and male infertility - An update.* Mitochondrion, 2020. **54**: p. 26-40.
5. Franca, M.M. and B.B. Mendonca, *Genetics of ovarian insufficiency and defects of folliculogenesis.* Best Pract Res Clin Endocrinol Metab, 2021: p. 101594.
6. Tiosano, D., J.A. Mears, and D.A. Buchner, *Mitochondrial Dysfunction in Primary Ovarian Insufficiency.* Endocrinology, 2019. **160**(10): p. 2353-2366.
7. Wang, T., et al., *Mitochondrial unfolded protein response gene Clpp is required to maintain ovarian follicular reserve during aging, for oocyte competence, and development of pre-implantation embryos.* Aging Cell, 2018. **17**(4): p. e12784.
8. Bhaskaran, S., et al., *Loss of mitochondrial protease ClpP protects mice from diet-induced obesity and insulin resistance.* EMBO Rep, 2018. **19**(3).
9. Newman, W.G., et al., *Perrault Syndrome*, in *GeneReviews((R))*, M.P. Adam, et al., Editors. 1993: Seattle (WA).
10. Faridi, R., et al., *New insights into Perrault syndrome, a clinically and genetically heterogeneous disorder.* Hum Genet, 2021.
11. Hochberg, I., et al., *Bi-allelic variants in the mitochondrial RNase P subunit PRORP cause mitochondrial tRNA processing defects and pleiotropic multisystem presentations.* Am J Hum Genet, 2021. **108**(11): p. 2195-2204.
12. Wawrzynow, A., et al., *The ClpX heat-shock protein of Escherichia coli, the ATP-dependent substrate specificity component of the ClpP-ClpX protease, is a novel molecular chaperone.* EMBO J, 1995. **14**(9): p. 1867-77.
13. Baker, T.A. and R.T. Sauer, *ClpXP, an ATP-powered unfolding and protein-degradation machine.* Biochim Biophys Acta, 2012. **1823**(1): p. 15-28.
14. Key, J., et al., *Inactivity of Peptidase ClpP Causes Primary Accumulation of Mitochondrial Disaggregase ClpX with Its Interacting Nucleoid Proteins, and of mtDNA.* Cells, 2021. **10**(12).
15. Torres-Odio, S., et al., *Loss of Mitochondrial Protease CLPP Activates Type I IFN Responses through the Mitochondrial DNA-cGAS-STING Signaling Axis.* J Immunol, 2021. **206**(8): p. 1890-1900.
16. Maletzko, A., et al., *Increased presence of nuclear DNAJA3 and upregulation of cytosolic STAT1 and of nucleic acid sensors trigger innate immunity in the ClpP-null mouse.* Neurogenetics, 2021. **22**(4): p. 297-312.
17. Key, J., et al., *Loss of mitochondrial ClpP, Lonp1, and Tfam triggers transcriptional induction of Rnf213, a susceptibility factor for moyamoya disease.* Neurogenetics, 2020. **21**(3): p. 187-203.
18. Granat, L., R.J. Hunt, and J.M. Bateman, *Mitochondrial retrograde signalling in neurological disease.* Philos Trans R Soc Lond B Biol Sci, 2020. **375**(1801): p. 20190415.
19. Monaghan, R.M. and A.J. Whitmarsh, *Mitochondrial Proteins Moonlighting in the Nucleus.* Trends Biochem Sci, 2015. **40**(12): p. 728-735.
20. Gewiss, R., T. Topping, and M.D. Griswold, *Cycles, waves, and pulses: Retinoic acid and the organization of spermatogenesis.* Andrology, 2020. **8**(4): p. 892-897.
21. Yao, J., et al., *Mouse testis transcriptome revealed using serial analysis of gene expression.* Mamm Genome, 2004. **15**(6): p. 433-51.
22. Klann, K., G. Tascher, and C. Munch, *Functional Translatome Proteomics Reveal Converging and Dose-Dependent Regulation by mTORC1 and eIF2alpha.* Mol Cell, 2020. **77**(4): p. 913-925 e4.
23. Robinson, M.D. and A. Oshlack, *A scaling normalization method for differential expression analysis of RNA-seq data.* Genome Biol, 2010. **11**(3): p. R25.

24. Baghirova, S., et al., *Sequential fractionation and isolation of subcellular proteins from tissue or cultured cells.* MethodsX, 2015. **2**: p. 440-5.
25. Llano, E., et al., *Shugoshin-2 is essential for the completion of meiosis but not for mitotic cell division in mice.* Genes Dev, 2008. **22**(17): p. 2400-13.
26. Faridi, R., et al., *Mutations of SGO2 and CLDN14 collectively cause coincidental Perrault syndrome.* Clin Genet, 2017. **91**(2): p. 328-332.
27. Clayton, S.A., et al., *Inflammation causes remodeling of mitochondrial cytochrome c oxidase mediated by the bifunctional gene C15orf48.* Sci Adv, 2021. **7**(50): p. eabl5182.
28. Lee, C.Q.E., et al., *Coding and non-coding roles of MOCCI (C15ORF48) coordinate to regulate host inflammation and immunity.* Nat Commun, 2021. **12**(1): p. 2130.
29. Xu, P., et al., *Structure, regulation, and (patho-)physiological functions of the stress-induced protein kinase CK1 delta (CSNK1D).* Gene, 2019. **715**: p. 144005.
30. Zaoui, K., et al., *ErbB2 receptor controls microtubule capture by recruiting ACF7 to the plasma membrane of migrating cells.* Proc Natl Acad Sci U S A, 2010. **107**(43): p. 18517-22.
31. Murakoshi, H., H. Wang, and R. Yasuda, *Local, persistent activation of Rho GTPases during plasticity of single dendritic spines.* Nature, 2011. **472**(7341): p. 100-4.
32. Liu, M., et al., *SHCBP1L, a conserved protein in mammals, is predominantly expressed in male germ cells and maintains spindle stability during meiosis in testis.* Mol Hum Reprod, 2014. **20**(6): p. 463-75.
33. Cahoon, C.K. and R.S. Hawley, *Regulating the construction and demolition of the synaptonemal complex.* Nat Struct Mol Biol, 2016. **23**(5): p. 369-77.
34. Dix, D.J., et al., *HSP70-2 is required for desynapsis of synaptonemal complexes during meiotic prophase in juvenile and adult mouse spermatocytes.* Development, 1997. **124**(22): p. 4595-603.
35. Dix, D.J., et al., *Targeted gene disruption of Hsp70-2 results in failed meiosis, germ cell apoptosis, and male infertility.* Proc Natl Acad Sci U S A, 1996. **93**(8): p. 3264-8.
36. Saju, J.M., et al., *Heat Shock Factor 5 Is Essential for Spermatogenesis in Zebrafish.* Cell Rep, 2018. **25**(12): p. 3252-3261 e4.
37. Yochem, J., et al., *Genetic analysis of two genes, dnaJ and dnaK, necessary for Escherichia coli and bacteriophage lambda DNA replication.* Mol Gen Genet, 1978. **164**(1): p. 9-14.
38. Ko, H.W., *The primary cilium as a multiple cellular signaling scaffold in development and disease.* BMB Rep, 2012. **45**(8): p. 427-32.
39. Falk, N., et al., *Specialized Cilia in Mammalian Sensory Systems.* Cells, 2015. **4**(3): p. 500-19.
40. Kumar, N. and A.K. Singh, *The anatomy, movement, and functions of human sperm tail: an evolving mystery.* Biol Reprod, 2021. **104**(3): p. 508-520.
41. Pivot-Pajot, C., et al., *Acetylation-dependent chromatin reorganization by BRDT, a testis-specific bromodomain-containing protein.* Mol Cell Biol, 2003. **23**(15): p. 5354-65.
42. Gaucher, J., et al., *Bromodomain-dependent stage-specific male genome programming by Brdt.* EMBO J, 2012. **31**(19): p. 3809-20.
43. Berkovits, B.D., et al., *The testis-specific double bromodomain-containing protein BRDT forms a complex with multiple spliceosome components and is required for mRNA splicing and 3'-UTR truncation in round spermatids.* Nucleic Acids Res, 2012. **40**(15): p. 7162-75.
44. Manterola, M., et al., *BRDT is an essential epigenetic regulator for proper chromatin organization, silencing of sex chromosomes and crossover formation in male meiosis.* PLoS Genet, 2018. **14**(3): p. e1007209.
45. Dhar, S., A. Thota, and M.R. Rao, *Insights into role of bromodomain, testis-specific (Brdt) in acetylated histone H4-dependent chromatin remodeling in mammalian spermiogenesis.* J Biol Chem, 2012. **287**(9): p. 6387-405.
46. Matzuk, M.M., et al., *Small-molecule inhibition of BRDT for male contraception.* Cell, 2012. **150**(4): p. 673-84.

47. Milenkovic, D., et al., *TWINKLE is an essential mitochondrial helicase required for synthesis of nascent D-loop strands and complete mtDNA replication.* Hum Mol Genet, 2013. **22**(10): p. 1983-93.
48. Jemt, E., et al., *Regulation of DNA replication at the end of the mitochondrial D-loop involves the helicase TWINKLE and a conserved sequence element.* Nucleic Acids Res, 2015. **43**(19): p. 9262-75.
49. Dennerlein, S., et al., *Human ERAL1 is a mitochondrial RNA chaperone involved in the assembly of the 28S small mitochondrial ribosomal subunit.* Biochem J, 2010. **430**(3): p. 551-8.
50. Tyynismaa, H., et al., *Twinkle helicase is essential for mtDNA maintenance and regulates mtDNA copy number.* Hum Mol Genet, 2004. **13**(24): p. 3219-27.
51. Meersseman, C., et al., *Bovine TWINKLE and mitochondrial ribosomal protein L43 genes are regulated by an evolutionary conserved bidirectional promoter.* Gene, 2014. **537**(1): p. 154-63.
52. Pierce, S.B., et al., *Mutations in mitochondrial histidyl tRNA synthetase HARS2 cause ovarian dysgenesis and sensorineural hearing loss of Perrault syndrome.* Proc Natl Acad Sci U S A, 2011. **108**(16): p. 6543-8.
53. Rossmanith, W., *Processing of human mitochondrial tRNA(Ser(AGY))GCU: a novel pathway in tRNA biosynthesis.* J Mol Biol, 1997. **265**(4): p. 365-71.
54. Karasik, A., C.A. Fierke, and M. Koutmos, *Interplay between substrate recognition, 5' end tRNA processing and methylation activity of human mitochondrial RNase P.* RNA, 2019. **25**(12): p. 1646-1660.
55. Kasimanickam, V. and R. Kasimanickam, *Exogenous retinoic acid and cytochrome P450 26B1 inhibitor modulate meiosis-associated genes expression in canine testis, an in vitro model.* Reprod Domest Anim, 2014. **49**(2): p. 315-23.
56. Soh, Y.Q., et al., *A Gene Regulatory Program for Meiotic Prophase in the Fetal Ovary.* PLoS Genet, 2015. **11**(9): p. e1005531.
57. Koubova, J., et al., *Retinoic acid activates two pathways required for meiosis in mice.* PLoS Genet, 2014. **10**(8): p. e1004541.
58. Buonomo, S.B., et al., *Disjunction of homologous chromosomes in meiosis I depends on proteolytic cleavage of the meiotic cohesin Rec8 by separin.* Cell, 2000. **103**(3): p. 387-98.
59. Chen, S., et al., *The role of REC8 in the innate immune response to viral infection.* J Virol, 2022: p. jvi0217521.
60. Larsson, N.G., et al., *A single mouse gene encodes the mitochondrial transcription factor A and a testis-specific nuclear HMG-box protein.* Nat Genet, 1996. **13**(3): p. 296-302.
61. Zhang, J., et al., *Acetylation of Smc3 by Eco1 is required for S phase sister chromatid cohesion in both human and yeast.* Mol Cell, 2008. **31**(1): p. 143-51.
62. Matilainen, O., P.M. Quiros, and J. Auwerx, *Mitochondria and Epigenetics - Crosstalk in Homeostasis and Stress.* Trends Cell Biol, 2017. **27**(6): p. 453-463.
63. Nikkanen, J., et al., *Mitochondrial DNA Replication Defects Disturb Cellular dNTP Pools and Remodel One-Carbon Metabolism.* Cell Metab, 2016. **23**(4): p. 635-48.
64. Kota, S.K. and R. Feil, *Epigenetic transitions in germ cell development and meiosis.* Dev Cell, 2010. **19**(5): p. 675-86.
65. Shetty, S. and U. Varshney, *Regulation of translation by one-carbon metabolism in bacteria and eukaryotic organelles.* J Biol Chem, 2021. **296**: p. 100088.
66. Hernandez-Hernandez, A., et al., *Chromatin structure contribution to the synaptonemal complex formation.* Cell Mol Life Sci, 2009. **66**(7): p. 1198-208.
67. Margalit, L., et al., *Trim24 and Trim33 Play a Role in Epigenetic Silencing of Retroviruses in Embryonic Stem Cells.* Viruses, 2020. **12**(9).
68. Lee, M.G., et al., *Physical and functional association of a trimethyl H3K4 demethylase and Ring6a/MBLR, a polycomb-like protein.* Cell, 2007. **128**(5): p. 877-87.
69. Crichton, J.H., C.J. Playfoot, and I.R. Adams, *The role of chromatin modifications in progression through mouse meiotic prophase.* J Genet Genomics, 2014. **41**(3): p. 97-106.

70. Tachibana, M., et al., *Functional dynamics of H3K9 methylation during meiotic prophase progression.* EMBO J, 2007. **26**(14): p. 3346-59.
71. Yi, S.J. and K. Kim, *Histone tail cleavage as a novel epigenetic regulatory mechanism for gene expression.* BMB Rep, 2018. **51**(5): p. 211-218.
72. Zhou, P., et al., *Histone cleavage as a mechanism for epigenetic regulation: current insights and perspectives.* Curr Mol Med, 2014. **14**(9): p. 1164-72.
73. Terada, Y., *Role of chromosomal passenger complex in chromosome segregation and cytokinesis.* Cell Struct Funct, 2001. **26**(6): p. 653-7.
74. Crosio, C., et al., *Mitotic phosphorylation of histone H3: spatio-temporal regulation by mammalian Aurora kinases.* Mol Cell Biol, 2002. **22**(3): p. 874-85.
75. Monen, J., et al., *Separase Cleaves the N-Tail of the CENP-A Related Protein CPAR-1 at the Meiosis I Metaphase-Anaphase Transition in C. elegans.* PLoS One, 2015. **10**(4): p. e0125382.
76. Wan, L., et al., *Translation stress and collided ribosomes are co-activators of cGAS.* Mol Cell, 2021. **81**(13): p. 2808-2822 e10.
77. Gao, M., et al., *cGAS/STING: novel perspectives of the classic pathway.* Mol Biomed, 2020. **1**(1): p. 7.
78. Zhao, B., et al., *The molecular basis of tight nuclear tethering and inactivation of cGAS.* Nature, 2020. **587**(7835): p. 673-677.
79. Banerjee, D., et al., *A non-canonical, interferon-independent signaling activity of cGAMP triggers DNA damage response signaling.* Nat Commun, 2021. **12**(1): p. 6207.
80. Li, T. and Z.J. Chen, *The cGAS-cGAMP-STING pathway connects DNA damage to inflammation, senescence, and cancer.* J Exp Med, 2018. **215**(5): p. 1287-1299.
81. Lu, B., et al., *Tid1 isoforms are mitochondrial DnaJ-like chaperones with unique carboxyl termini that determine cytosolic fate.* J Biol Chem, 2006. **281**(19): p. 13150-13158.
82. Rackham, O., et al., *Pentatricopeptide repeat domain protein 1 lowers the levels of mitochondrial leucine tRNAs in cells.* Nucleic Acids Res, 2009. **37**(17): p. 5859-67.
83. Sanchez, M.I., et al., *RNA processing in human mitochondria.* Cell Cycle, 2011. **10**(17): p. 2904-16.
84. Uittenbogaard, M. and A. Chiaramello, *Novel subcellular localization of the DNA helicase Twinkle at the kinetochore complex during mitosis in neuronal-like progenitor cells.* Histochem Cell Biol, 2016. **145**(3): p. 275-86.
85. Nikali, K., et al., *Infantile onset spinocerebellar ataxia is caused by recessive mutations in mitochondrial proteins Twinkle and Twinky.* Hum Mol Genet, 2005. **14**(20): p. 2981-90.
86. Oka, Y., et al., *UBL5 is essential for pre-mRNA splicing and sister chromatid cohesion in human cells.* EMBO Rep, 2014. **15**(9): p. 956-64.
87. Rinaldi, V.D., et al., *The DNA Damage Checkpoint Eliminates Mouse Oocytes with Chromosome Synapsis Failure.* Mol Cell, 2017. **67**(6): p. 1026-1036 e2.
88. Nakada, K., et al., *Mitochondria-related male infertility.* Proc Natl Acad Sci U S A, 2006. **103**(41): p. 15148-53.
89. Jiang, M., et al., *Increased Total mtDNA Copy Number Cures Male Infertility Despite Unaltered mtDNA Mutation Load.* Cell Metab, 2017. **26**(2): p. 429-436 e4.
90. Lee, W.R., et al., *Transcriptomic analysis of mitochondrial TFAM depletion changing cell morphology and proliferation.* Sci Rep, 2017. **7**(1): p. 17841.
91. Chen, S., et al., *The Role of REC8 in the Innate Immune Response to Viral Infection.* J Virol, 2022. **96**(6): p. e0217521.
92. Fu, X.F., et al., *DAZ Family Proteins, Key Players for Germ Cell Development.* Int J Biol Sci, 2015. **11**(10): p. 1226-35.
93. Jiao, X., P. Trifillis, and M. Kiledjian, *Identification of target messenger RNA substrates for the murine deleted in azoospermia-like RNA-binding protein.* Biol Reprod, 2002. **66**(2): p. 475-85.
94. Li, H., et al., *DAZL is a master translational regulator of murine spermatogenesis.* Natl Sci Rev, 2019. **6**(3): p. 455-468.

95. Gao, X., et al., *A G-quadruplex DNA structure resolvase, RHAU, is essential for spermatogonia differentiation.* Cell Death Dis, 2015. **6**: p. e1610.
96. Cheng, X., et al., *PDIP38 associates with proteins constituting the mitochondrial DNA nucleoid.* J Biochem, 2005. **138**(6): p. 673-8.
97. Wong, A., et al., *PDIP38 is translocated to the spliceosomes/nuclear speckles in response to UV-induced DNA damage and is required for UV-induced alternative splicing of MDM2.* Cell Cycle, 2013. **12**(19): p. 3184-93.
98. Zhang, L.S., et al., *ALKBH7-mediated demethylation regulates mitochondrial polycistronic RNA processing.* Nat Cell Biol, 2021. **23**(7): p. 684-691.
99. Kiat, L.S., K.M. Hui, and G. Gopalan, *Aurora-A kinase interacting protein (AIP), a novel negative regulator of human Aurora-A kinase.* J Biol Chem, 2002. **277**(47): p. 45558-65.
100. Koc, E.C., et al., *Identification and characterization of CHCHD1, AURKAIP1, and CRIF1 as new members of the mammalian mitochondrial ribosome.* Front Physiol, 2013. **4**: p. 183.
101. Katayama, H., et al., *Aurora-A kinase phosphorylation of Aurora-A kinase interacting protein (AIP) and stabilization of the enzyme-substrate complex.* J Cell Biochem, 2007. **102**(5): p. 1318-31.
102. Nguyen, A.L., et al., *Genetic Interactions between the Aurora Kinases Reveal New Requirements for AURKB and AURKC during Oocyte Meiosis.* Curr Biol, 2018. **28**(21): p. 3458-3468 e5.
103. Musacchio, A. and E.D. Salmon, *The spindle-assembly checkpoint in space and time.* Nat Rev Mol Cell Biol, 2007. **8**(5): p. 379-93.
104. Dieterich, K., et al., *Homozygous mutation of AURKC yields large-headed polyploid spermatozoa and causes male infertility.* Nat Genet, 2007. **39**(5): p. 661-5.
105. Bertolin, G. and M. Tramier, *Insights into the non-mitotic functions of Aurora kinase A: more than just cell division.* Cell Mol Life Sci, 2020. **77**(6): p. 1031-1047.
106. Deutsch, E.W., et al., *The ProteomeXchange consortium in 2020: enabling 'big data' approaches in proteomics.* Nucleic Acids Res, 2020. **48**(D1): p. D1145-D1152.
107. Keelagher, R.E., et al., *Separable roles for Exonuclease I in meiotic DNA double-strand break repair.* DNA Repair (Amst), 2011. **10**(2): p. 126-37.
108. Ferguson, R.L., G. Pascreau, and J.L. Maller, *The cyclin A centrosomal localization sequence recruits MCM5 and Orc1 to regulate centrosome reduplication.* J Cell Sci, 2010. **123**(Pt 16): p. 2743-9.
109. Bommi, J.R., et al., *Meiosis-specific cohesin component, Rec8, promotes the localization of Mps3 SUN domain protein on the nuclear envelope.* Genes Cells, 2019. **24**(1): p. 94-106.
110. Hori, A., et al., *The conserved Wdr8-hMsd1/SSX2IP complex localises to the centrosome and ensures proper spindle length and orientation.* Biochem Biophys Res Commun, 2015. **468**(1-2): p. 39-45.
111. Zhang, B., et al., *GSK3beta-Dzip1-Rab8 cascade regulates ciliogenesis after mitosis.* PLoS Biol, 2015. **13**(4): p. e1002129.
112. Wu, Z., et al., *CEP290 is essential for the initiation of ciliary transition zone assembly.* PLoS Biol, 2020. **18**(12): p. e3001034.
113. Wang, X., et al., *Mitotic regulator SKAP forms a link between kinetochore core complex KMN and dynamic spindle microtubules.* J Biol Chem, 2012. **287**(47): p. 39380-90.

Preprints (www.preprints.org) | NOT PEER-REVIEWED | Posted: 27 April 2022 doi:10.20944/preprints202204.0245.v1

Supplementary Materials

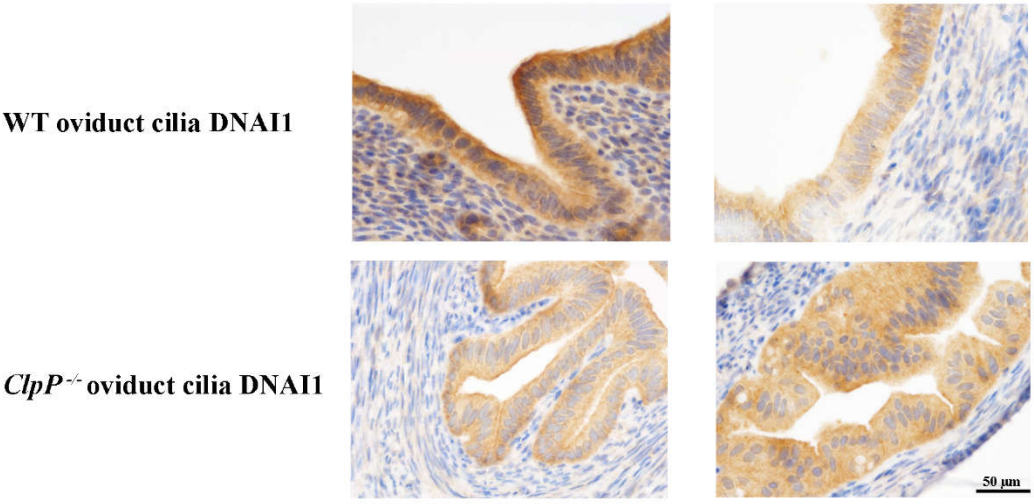

Figure S1. Immunohistochemistry of ClpP-null oviduct. Immunofluorescence staining for DNAI1 of female WT and ClpP-null mouse Fallopian tubes revealed no difference in the detection of this cilia-specific protein.

Preprints (www.preprints.org) | NOT PEER-REVIEWED | Posted: 27 April 2022 doi:10.20944/preprints202204.0245.v1

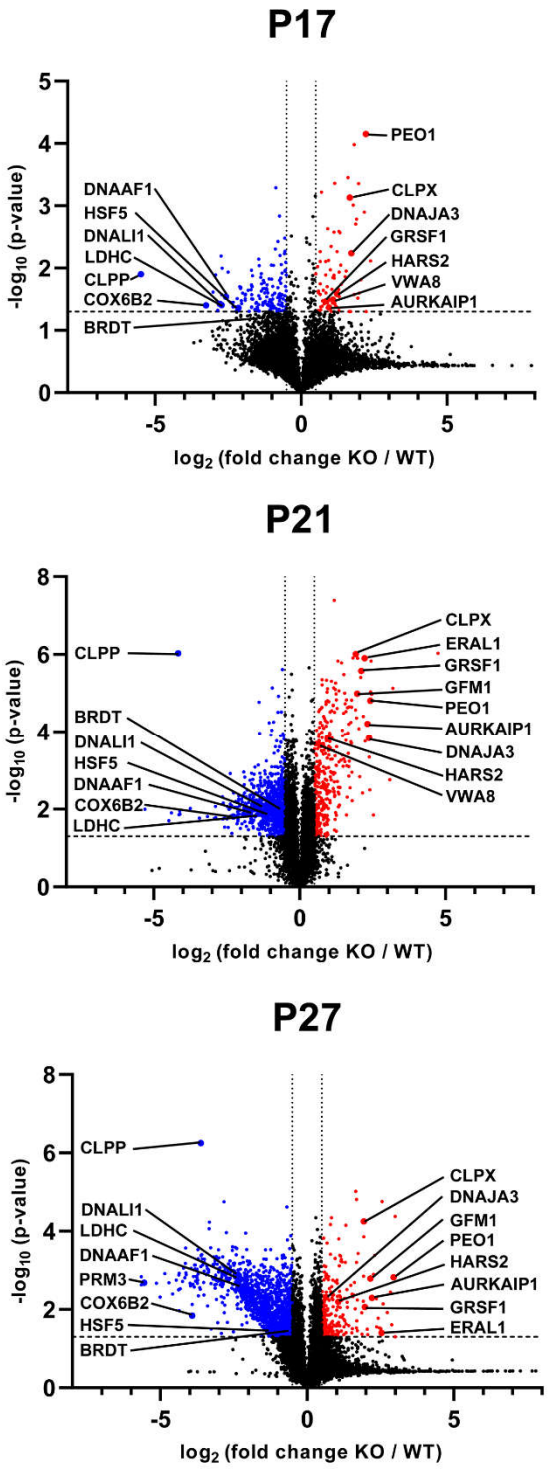

Figure S2. ClpP-null testis global proteome volcano plots at three ages. During the first round of spermatogenesis, there is complete synchronization of maturation stages. At P17, when early spermatocytes are terminating meiosis-I, several putative ClpXP substrate proteins in mitochondria such as PEO1, DNAJA3, AURKAIP1, and VWA8 are already accumulated, while mitochondrial bioenergetic deficits are reflected by reduced abundance for COX6B2 and LDHC. Curiously, already at this stage, the chaperone-controlling transcription factor HSF5 is repressed, and the supply of axonemal dynein factors such as DNAAF1 and DNALI1 is deficient long before tail formation is initiated. At P21 around the end of meiosis-II, these above dysregulations are observed again, but many additional dysregulations appear. At P27, the number of strong downregulations increases massively, e.g. a >30-fold reduction in protamine PRM3 levels, mirroring the absence of elongated spermatids. .

Preprints (www.preprints.org) | NOT PEER-REVIEWED | Posted: 27 April 2022 doi:10.20944/preprints202204.0245.v1

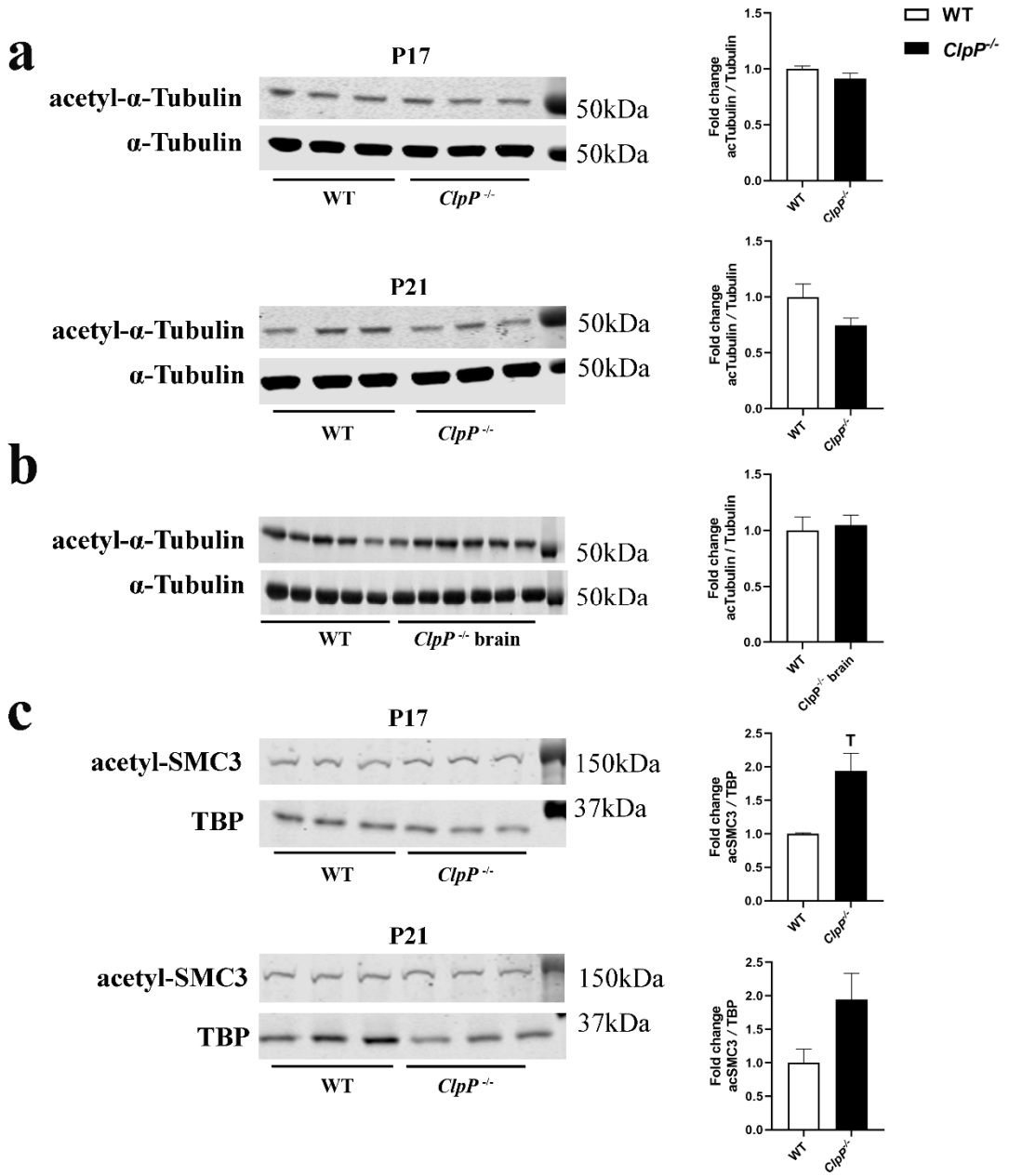

Figure S3. Quantitative immunoblots to validate proteome profile. (a) Analysis of acetyl-α-Tubulin in testis at P17 (upper membrane) and P21 (lower membrane) revealed no differences at these early developmental stages. **(b)** Analysis of acetyl-α-Tubulin in brain tissue of 12-month-old WT (n=5) and ClpP$^{-/-}$ (n=6) mice revealed no differences. **(c)** Quantitative immunoblots for acetyl-SMC3 showed increased of acSMA3 already at P17 and P21, consistent with Figure 3c but without significance due to low sample number. T $0.05 < p < 0.1$.

Preprints (www.preprints.org) | NOT PEER-REVIEWED | Posted: 27 April 2022 doi:10.20944/preprints202204.0245.v1

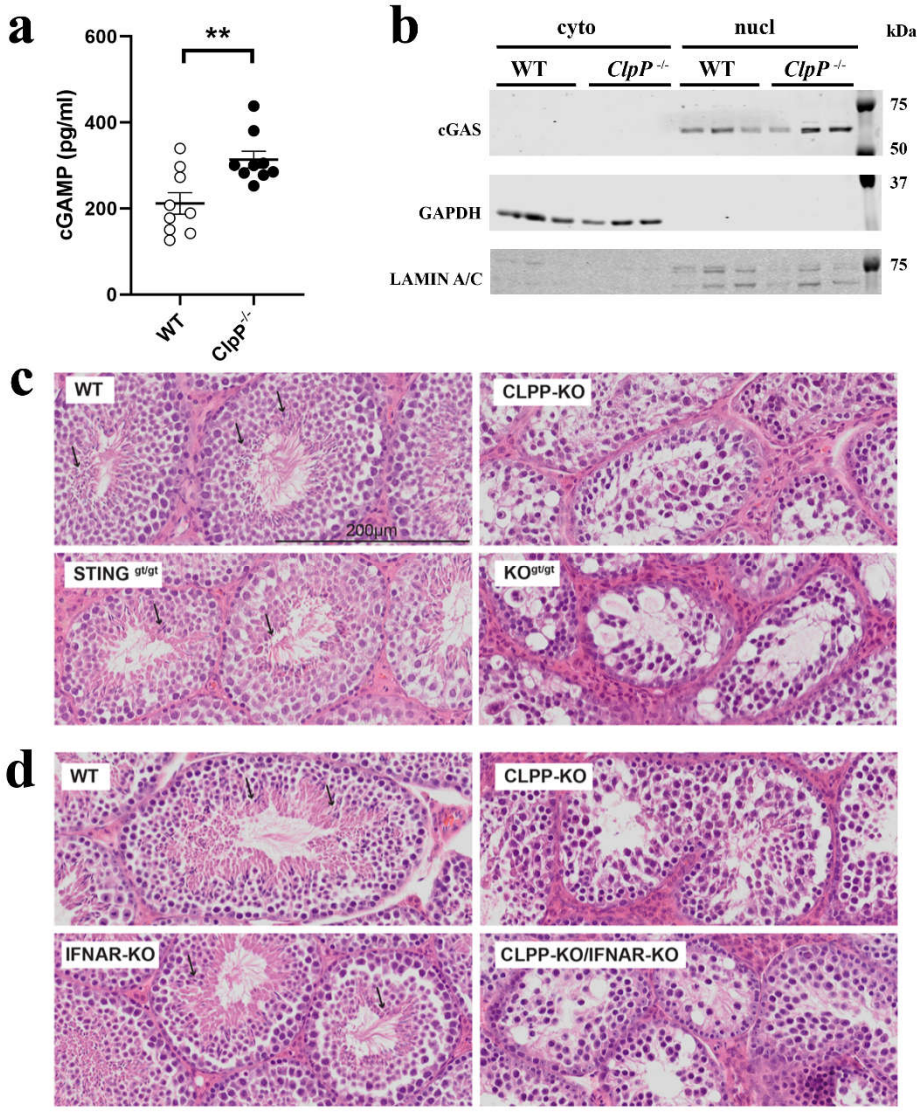

Figure S4. (a) ELISA quantification of adult testis homogenate cGAMP levels (n=9, ** $p < 0.01$); **(b)** immunoblot of cGAS in cytosolic versus nuclear P21 testis fractions (n=3). Upon light microscopy assessment of testis H&E stains, the azoospermia of ClpP-null mice was not rescued by additional **(c)** STING-deletion or **(d)** IFNAR-deletion.

Preprints (www.preprints.org) | NOT PEER-REVIEWED | Posted: 27 April 2022 doi:10.20944/preprints202204.0245.v1

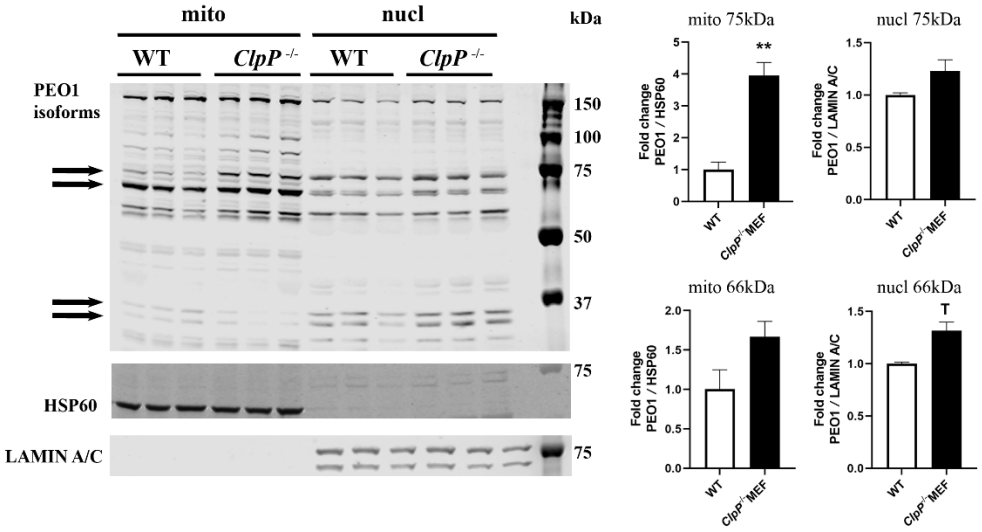

Figure S5. PEO1 isoforms in ClpP-null MEF fractions. Mitochondrial fraction (left margin) probed with anti-PEO1 C-terminal antibody showed accumulation of the putative 66 kDa band for Twinkle and of the putative 60 kDa band for Twinky in mutant samples, while bands of 32 kDa and 25 kDa size (that correspond to PEO1 isoforms reported in UniProt database) were decreased. In the ClpP-null MEF nuclear fraction (right margin), these four PEO1-immunoreactive bands appeared to accumulate. T $0.05 < p < 0.1$; ** $p < 0.01$.

Table S1. ClpP-null testis transcript upregulations at age 9-10 months. Spermatogenesis factors were selected here and ranked by fold-change. The columns provide the oligonucleotide ID under analysis, the mRNA gene symbol under study, the nominal p-value, the actual p-value after correction for multiple testing, the M-value (log2 of fold-change, visualized as a gradient of green shading), and the relevant mouse transcript isoform. Two additional columns complement these data, adding literature knowledge regarding the functional context of these factors, and regarding their appearance at different sperm maturation stages (blue background highlights early events). Most components of the condensin/cohesin/synaptonemal/strand-invasion/mismatch-repair/HR complexes show upregulation, as well as some components of the anaphase promoting complex. Particularly strong effects concern *Cenpa*, a centromere-specific homolog of histone H3 that is regulated by proteolytic cleavage [72, 75], and the meiotic DNA mismatch repair enzyme *Exo1* [107].

ID	Gene Symbol	P.Value	adj. P Value	KO - WT testis	Transcript ID	Acts in	differentiation Marker
1417947_PM_at	**Pcna**	0.001918	0.00486	0.6386156	Mm.7141.1	homologous recombination	early spermatocytes
1417831_PM_at	**Smc1a**	0.000398	0.0012	0.681299	Mm.26412.1	cohesion of sister chromatids	early spermatocytes
1454952_PM_s_at	**Ncapd3**	0.001459	0.00381	0.6915202	Mm.21448.1	condensin complex	early spermatocytes
1431921_PM_a_at	**Stag1**	0.002939	0.00709	0.7123757	Mm.42135.2	cohesion of sister chromatids	early spermatocytes
1415707_PM_at	**Anapc2**	0.000537	0.00157	0.7303582	Mm.202841.1	anaphase promoting complex/	spermatogonia to early spermatocytes
1422630_PM_at	**Rad50**	0.000884	0.00245	0.7490552	Mm.4888.1	homologous recombination	early spermatocytes
1423920_PM_at	**Ncaph**	0.000908	0.00251	0.8050998	Mm.29786.1	condensin complex	early spermatocytes
1420441_PM_at	**Cenpc1**	0.000103	0.00036	0.8078997	Mm.4649.1	centromere	early spermatocytes
1439510_PM_at	**Sgol1**	5.43E-05	0.0002	0.8179663	Mm.188453.1	cohesion of sister chromatids	early spermatocytes
1444271_PM_at	**Anapc1**	0.003729	0.00873	0.8431961	Mm.132986.1	anaphase promoting complex/	spermatogonia to early spermatocytes
1426846_PM_at	**Cenpt**	0.003907	0.0091	0.8440046	Mm.28323.1	centromere	?
1418458_PM_at	**Anapc7**	3.03E-06	1.55E-05	0.8487623	Mm.18805.1	anaphase promoting complex/	spermatogonia to early spermatocytes

Preprints (www.preprints.org) | NOT PEER-REVIEWED | Posted: 27 April 2022 doi:10.20944/preprints202204.0245.v1

1422016_PM_a_at	**Cenph**	0.000125	0.00043	0.8518894	Mm.181792.1	centromere	?
1418919_PM_at	**Sgol1**	0.000805	0.00226	0.8776233	Mm.153202.1	cohesion of sister chromatids	early spermatocytes
1449537_PM_at	**Msh5**	0.001745	0.00447	0.9090713	Mm.24192.1	homologous recombination	early spermatocytes
1427062_PM_at	**Rbbp8**	0.000685	0.00195	0.9113928	Mm.29216.1	homologous recombination	early spermatocytes
1452606_PM_at	**Mnd1**	1.63E-05	6.94E-05	0.9227692	Mm.177053.1	homologous recombination	early spermatocytes
1424324_PM_at	**Esco1**	6.11E-07	3.77E-06	0.9480059	Mm.21177.1	cohesion of sister chromatids	early spermatocytes
1426666_PM_a_at	**Sun1**	3.83E-05	0.00015	0.9511082	Mm.23889.1	synaptonemal complex	early spermatocytes
1448314_PM_at	**Cdk1**	0.00086	0.00239	0.9534518	Mm.4761.1	chromosome condensation	early spermatocytes
1435739_PM_at	**Lats1**	2.56E-06	1.34E-05	0.9582136	Mm.34083.1	acrosome head	
1449338_PM_at	**Anapc16**	1.54E-08	1.51E-07	0.9728152	Mm.21793.1	anaphase promoting complex/	spermatogonia to early spermatocytes
1416915_PM_at	**Msh6**	6.55E-05	0.00024	0.9857101	Mm.18210.1	homologous recombination	early spermatocytes
1450420_PM_at	**Stag1**	4.64E-05	0.00018	1.0021919	Mm.42135.1	cohesion of sister chromatids	early spermatocytes
1429477_PM_at	**Ncaph2**	3.81E-06	1.91E-05	1.0120139	Mm.100466.1	condensin complex	early spermatocytes
1419994_PM_s_at	**Anapc16**	1.94E-07	1.39E-06	1.0134921	Mm.195418.1	anaphase promoting complex/	spermatogonia to early spermatocytes
1435242_PM_at	**Pds5b**	1.14E-05	5.04E-05	1.0203758	Mm.22645.1	cohesion of sister chromatids	early spermatocytes
1435177_PM_a_at	**Anapc5**	1.58E-05	6.75E-05	1.0783799	Mm.45312.4	anaphase promoting complex/	spermatogonia to early spermatocytes
1423930_PM_at	**Anapc4**	2.37E-06	1.25E-05	1.0797619	Mm.27142.1	anaphase promoting complex/	spermatogonia to early spermatocytes
1421940_PM_at	**Stag1**	8.20E-06	3.77E-05	1.1063719	Mm.42135.1	cohesion of sister chromatids	early spermatocytes
1444122_PM_at	**Sycp2**	1.27E-05	5.56E-05	1.1120346	Mm.103203.1	synaptonemal complex	early spermatocytes
1449534_PM_at	**Sycp3**	2.11E-07	1.50E-06	1.1735701	Mm.148209.1	synaptonemal complex	early spermatocytes
1441238_PM_at	**Pds5a**	0.00127	0.00338	1.2141413	Mm.103018.1	cohesion of sister chromatids	early spermatocytes
1417926_PM_at	**Ncapg2**	8.52E-07	5.04E-06	1.2545235	Mm.21516.1	condensin complex	early spermatocytes
1434189_PM_at	**Stag1**	3.25E-08	2.90E-07	1.2803068	Mm.145100.1	cohesion of sister chromatids	early spermatocytes
1419838_PM_s_at	**Plk4**	6.38E-08	5.22E-07	1.2877845	Mm.198533.1	centriole duplication	
1421939_PM_a_at	**Stag1**	2.98E-07	2.02E-06	1.3715147	Mm.42135.1	cohesion of sister chromatids	early spermatocytes
1435178_PM_x_at	**Anapc5**	3.59E-10	5.97E-09	1.3847976	Mm.45312.4	anaphase promoting complex/	spermatogonia to early spermatocytes
1426270_PM_at	**Smc5**	2.31E-07	1.62E-06	1.3960858	Mm.23267.1	cohesion of sister chromatids	early spermatocytes
1416161_PM_at	**Rad21**	2.24E-10	3.97E-09	1.4012767	Mm.182628.1	cohesion of sister chromatids	early spermatocytes
1423931_PM_s_at	**Anapc4**	1.03E-10	2.05E-09	1.4135815	Mm.27142.1	anaphase promoting complex/	spermatogonia to early spermatocytes
1453307_PM_a_at	**Anapc5**	1.33E-06	7.49E-06	1.4365563	Mm.45312.2	anaphase promoting complex/cyclosome	spermatogonia to early spermatocytes
1417830_PM_at	**Smc1a**	5.51E-08	4.60E-07	1.4664107	Mm.26412.1	cohesion of sister chromatids	early spermatocytes
1434443_PM_at	**Anapc1**	2.12E-07	1.50E-06	1.4804799	Mm.200869.1	anaphase promoting complex/cyclosome	spermatogonia to early spermatocytes

Preprints (www.preprints.org) | NOT PEER-REVIEWED | Posted: 27 April 2022 doi:10.20944/preprints202204.0245.v1

1434444_PM_s_at	**Anapc1**	8.05E-08	6.40E-07	1.4843055	Mm.200869.1	anaphase promoting complex/	spermatogonia to early spermatocytes
1429557_PM_at	**Mcm8**	2.67E-06	1.39E-05	1.4903992	Mm.45710.1	MCM5; replicative helicase at centro-some	?
1418281_PM_at	**Rad51**	1.91E-08	1.83E-07	1.5028384	Mm.231.1	homologous recombination	early spermatocytes
1456695_PM_x_at	**Anapc5**	3.85E-11	8.64E-10	1.5183742	Mm.45312.8	anaphase promoting complex/	spermatogonia to early spermatocytes
1433822_PM_x_at	**Anapc5**	1.01E-09	1.45E-08	1.5259569	Mm.45312.3	anaphase promoting complex/	spermatogonia to early spermatocytes
1449819_PM_at	**Dmc1**	4.11E-10	6.71E-09	1.544186	Mm.2524.1	homologous recombination	early spermatocytes
1416906_PM_at	**Anapc5**	1.40E-10	2.67E-09	1.5482041	Mm.45312.1	anaphase promoting complex/cyclosome	spermatogonia to early spermatocytes
1421183_PM_at	**Tex12**	1.37E-07	1.02E-06	1.5482041	Mm.78133.1	synaptonemal complex	early spermatocytes
1417570_PM_at	**Anapc1**	4.47E-08	3.82E-07	1.5614718	Mm.3989.1	anaphase promoting complex/	spermatogonia to early spermatocytes
1428304_PM_at	**Esco2**	3.90E-07	2.54E-06	1.5855591	Mm.46440.1	cohesion of sister chromatids	early spermatocytes
1415680_PM_at	**Anapc1**	1.23E-10	2.39E-09	1.5858782	Mm.3989.1	anaphase promoting complex/cyclosome	spermatogonia to early spermatocytes
1436161_PM_at	**Pds5b**	4.85E-07	3.07E-06	1.5892788	Mm.127302.1	cohesion of sister chromatids	early spermatocytes
1420568_PM_at	**Stra8**	7.40E-11	1.53E-09	1.7173137	Mm.5171.1	CENPX; centromere	?
1429787_PM_x_at	**Zwint**	2.17E-05	8.99E-05	1.7974157	Mm.38994.3	kinetochore	
1417960_PM_at	**Cpeb1**	8.53E-07	5.04E-06	1.877204	Mm.22062.1	synaptonemal complex	early spermatocytes
1421849_PM_at	**Stag2**	8.43E-11	1.71E-09	1.9144172	Mm.24025.1	cohesion of sister chromatids	early spermatocytes
1450842_PM_a_at	**Cenpa**	1.26E-09	1.76E-08	1.9975163	Mm.6579.1	centromere	?
1418026_PM_at	**Exo1**	3.16E-11	7.26E-10	2.174443	Mm.34988.1	homologous recombination	early spermatocytes

Table S2. ClpP-null testis transcript downregulations at age 9-10 months. Spermatogenesis factors were selected here and ranked by fold-change. The columns provide the oligonucleotide ID under analysis, the mRNA gene symbol under study, the nominal p-value, the actual p-value after correction for multiple testing, the M-value (log2 of fold-change, visualized as a gradient of green shading), and the relevant mouse transcript isoform. Two additional columns complement these data, adding literature knowledge regarding the functional context of these factors, and regarding their appearance at different sperm maturation stages (blue background highlights early events). Among the milder downregulations at the upper end, the replicative DNA helicase *Ccdc46* (encoding MCM5) and the spindle anchor *Ssx2ip*, which have established functions at the centrosome [108-110], exhibit exceptional transcript downregulations among early spermatocyte pathways, while all other early factors reflect reduced chromatid separation by the spindle poles. The only exception might be the downregulation of *Dzip1*, which is considered a pre-meiotic factor, but there are reports implicating this protein also in the subsequent ciliogenesis stage [111, 112]. Considering in detail the strong downregulations, it was noteworthy that the mRNA levels of *Spata18* (which encodes a protein responsible for the mitophagic elimination of mitochondria before the rearrangement of remaining mitochondria in the midpiece of elongating spermatids) and *Odf1* (a component of outer dense fibers surrounding mitochondria in the midpiece of spermatids) were affected to a similar degree as *Spem1* (responsible for the cytoplasm elimination in elongating spermatids), *1110017D15Rik* (responsible for the manchette of elongating spermatids), *4430402I18Rik* (responsible for the connecting piece of spermatids), *Poc1b* (responsible for the axoneme base of elongating spermatids), and *Sun5* (responsible for acrosome biogenesis in spermatids). Thus, in elongating spermatids the factors relevant for mitochondria are not exceptionally dysregulated but instead are part of a global massive reduction that may reflect the complete loss of elongated spermatids. The only factor with similarly massive downregulation that has a role much earlier at

Preprints (www.preprints.org) | NOT PEER-REVIEWED | Posted: 27 April 2022 doi:10.20944/preprints202204.0245.v1

the kinetochore as an essential spindle component during meiotic anaphase [113] was *D2Ertd750e* (encoding Kinastrin, also known as SKAP).

Oligonucleotide ID	Gene Symbol	P Value	adj. P Value	KO - WT testis	Transcript ID	Acts in	differentiation marker
1417239_PM_at	**Cetn3**	0.000589	0.001705	-0.6263	Mm.12481.1	microtubule-organizing center structure	?
1416553_PM_at	**Stra13**	0.00171	0.004388	-0.6769	Mm.73550.1	CENPX; centromere	?
1447278_PM_at	**Cep164**	0.002952	0.007114	-0.8106	Mm.213896.1	chromosome segregation; ciliary targeting	spermatogonia, spermatocytes and spermatids
1455609_PM_at	**Cit**	0.000194	0.000635	-0.8283	Mm.23631.1	central spindle, cytokinesis	early spermatocytes
1450396_PM_at	**Stag2**	0.004035	0.009355	-0.8824	Mm.24025.1	cohesion of sister chromatids	?
1428706_PM_at	**Cenpv**	0.000105	0.000366	-0.8919	Mm.25170.1	centromere	?
1424278_PM_a_at	**Birc5**	1.90E-05	7.96E-05	-0.9227	Mm.8552.2	SURVIVIN; chromosome passenger complex	early spermatocytes
1429376_PM_s_at	**Anapc10**	2.72E-06	1.41E-05	-0.9327	Mm.18790.1	anaphase promoting complex/cyclosome	spermatogonia to early spermatocytes
1417326_PM_a_at	**Anapc11**	1.64E-07	1.20E-06	-0.9646	Mm.21645.1	anaphase promoting complex/cyclosome	?
1416309_PM_at	**Nusap1**	0.00016	0.000535	-0.9931	Mm.27584.1	chromosomes and spindles	?
1452499_PM_a_at	**Kif2a**	7.70E-06	3.57E-05	-1.0678	Mm.4415.3	bipolar mitotic spindles	?
1424978_PM_at	**Odf4**	10.92151	1.02E-05	-1.1617	Mm.76826.1	outer dense fiber	spermatids
1423203_PM_a_at	**Cetn1**	1.03E-05	4.62E-05	-1.1801	Mm.195831.1	microtubule-organizing center	spermatids
1427079_PM_at	**Mapre3**	0.003118	0.007468	-1.202	Mm.22628.1	anchors microtubules at centrosome	?
1424511_PM_at	**Aurka**	8.97E-06	4.09E-05	-1.2271	Mm.11738.1	centrosome duplication, spindle assembly	spermatogonia, spermatocytes and spermatids
1432511_PM_s_at	**Haus2**	3.33E-07	2.21E-06	-1.2572	Mm.195672.1	centrosome integrity, spindle assembly	?
1421235_PM_s_at	**Recql5**	3.22E-06	1.64E-05	-1.3266	Mm.105253.1	chromosome separation after crossover	until early spermatocytes
1456097_PM_a_at	**Itgb3bp**	2.56E-07	1.77E-06	-1.3925	Mm.64982.2	assembly of kineto-chore at centromere	?
1460199_PM_a_at	**Pafah1b1**	2.24E-07	1.57E-06	-1.4546	Mm.56337.1	translocates nucleus towards centrosome	spermatogonia, spermatocytes and spermatids
1434119_PM_at	**D2Wsu81e**	1.10E-06	6.30E-06	-1.471	Mm.4449.2	CENP32; centrosome, kinetochore	early spermatocytes
1452792_PM_at	**Dzip1**	2.70E-07	1.85E-06	-1.5162	Mm.87456.2	DAZL interaction, cilium formation	premeiotic spermatogonia
1443772_PM_at	**Dzip1**	1.69E-09	2.27E-08	-1.8706	Mm.207848.1	DAZL interaction, cilium formation	premeiotic spermatogonia
1449358_PM_at	**M1ap**	4.71E-09	5.51E-08	-1.8725	Mm.100652.1	required for meiosis-I progression, crosso-ver	until late spermatocytes
1449364_PM_at	**Aurkc**	4.23E-09	5.04E-08	-1.9749	Mm.12877.1	chromosome alignment/separation, spindles	until late spermatocytes
1450662_PM_at	**Tesk1**	2.93E-08	2.66E-07	-2.0749	Mm.10154.1	at and after the mei-otic phase	late spermatocytes, round spermatids
1430847_PM_a_at	**Crem**	2.12E-10	3.80E-09	-2.0996	Mm.220180.1	spermiogenesis transcription	from round spermatids
1439918_PM_at	**Odf2**	35.27699	1.00E-10	-2.2554	Mm.179350.1	outer dense fiber	spermatids
1428825_PM_at	**Nr6a1**	3.24E-13	1.40E-11	-2.3854	Mm.44282.1	spermiogenesis transcription	from round spermatids
1429303_PM_at	**Klf17**	3.36E-10	5.64E-09	-2.389	Mm.3848.1	spermiogenesis transcription	round spermatids

Preprints (www.preprints.org) | NOT PEER-REVIEWED | Posted: 27 April 2022 doi:10.20944/preprints202204.0245.v1

1435216_PM_a_at	**Odf2**	8.454669	7.74E-05	-2.4325	Mm.663.3	outer dense fiber	spermatids
1421657_PM_a_at	**Sox17**	1.56E-11	3.99E-10	-2.4654	Mm.5080.1	pre/post-meiotic transcription	early spermato-cytes to round spermatids
1439666_PM_at	**Odf3b**	26.86855	1.91E-09	-2.5295	Mm.46278.1	outer dense fiber	spermatids
1448191_PM_at	**Plk1**	6.04E-14	3.37E-12	-2.5371	Mm.16525.1	cohesin removing, anaphase promoting	early spermato-cytes to round spermatids
1428826_PM_at	**Nr6a1**	3.20E-10	5.40E-09	-2.565	Mm.44282.1	spermiogenesis transcription	from round spermatids
1426040_PM_a_at	**Odf2**	8.645987	6.54E-05	-2.6075	Mm.663.2	outer dense fiber	spermatids
1428968_PM_at	**Cep57**	7.47E-12	2.12E-10	-2.622	Mm.157212.1	Tsp57; centrosome	round spermatids
1427590_PM_at	**Zfp39**	1.79E-10	3.27E-09	-2.7465	Mm.127646.1	pre/post-meiotic transcription	spermatocytes and spermatids
1430076_PM_at	**Ccdc116**	1.84E-15	1.93E-13	-3.0959	Mm.101656.1	centrosome	ejaculated sperm
1417514_PM_at	**Ssx2ip**	2.29E-11	5.51E-10	-3.2826	Mm.200783.1	centrosome maturation, spindle poles	early spermatocytes
1418650_PM_at	**Spata6**	6.76E-09	7.48E-08	-3.3413	Mm.8540.1	formation of connecting piece	spermatids
1419147_PM_at	**Rec8**	1.78E-10	3.25E-09	-3.477	Mm.23149.1	cohesion of sister chromatids & centro-mere	spermatocytes and spermatids
1432522_PM_s_at	**Ccdc46**	4.16E-11	9.22E-10	-3.6213	Mm.200758.1	MCM5; replicative helicase at centro-some	?
1456866_PM_x_at	**1700027D21Rik**	1.03E-15	1.20E-13	-3.7024	Mm.45613.1	SPATC1L; centriole	neck region of sperm
1449391_PM_at	**Zfp37**	1.19E-12	4.32E-11	-3.8232	Mm.5011.1	spermiogenesis transcription	elongating spermatids
1429032_PM_at	**Micalcl**	5.56E-14	3.13E-12	-3.8363	Mm.37406.1	Rab effector	round spermatids to spermatozoa
1424218_PM_a_at	**Creb3l4**	2.71E-12	8.82E-11	-3.9317	Mm.23341.1	ATCE1; acrosome associated	spermatids
1456555_PM_at	**Ccdc67**	4.54E-11	9.98E-10	-3.9453	Mm.32237.1	centriole amplification	?
1429912_PM_at	**Sun5**	2.87E-12	9.25E-11	-4.0224	Mm.33629.1	acrosome biogenesis	round spermatid
1429414_PM_at	**D7Ertd443e**	5.91E-17	1.29E-14	-4.1241	Mm.87451.1	centriole assembly, spindle /cilia for-mation	?
1443670_PM_at	**Odf3b**	81.79207	5.85E-15	-4.1424	Mm.46278.2	outer dense fiber	spermatids
1420081_PM_s_at	**D2Ertd750e**	6.53E-20	9.17E-17	-4.1533	Mm.195223.1	KNSTRN; kinetochore, promotes anaphase	spermatogonia to spermatocytes
1441916_PM_s_at	**Odf3**	46.42885	4.55E-12	-4.276	Mm.36221.1	outer dense fiber	spermatids
1429325_PM_at	**Poc1b**	1.28E-18	6.01E-16	-4.3802	Mm.56455.1	centriole assembly, spindle /cilia for-mation	spermatid axoneme base
1443671_PM_x_at	**Odf3b**	87.46212	2.61E-15	-4.4309	Mm.46278.2	outer dense fiber	spermatids
1422585_PM_at	**Odf1**	26.32088	2.37E-09	-4.48	Mm.9397.1	outer dense fiber	spermatids
1420446_PM_at	**Odf3**	36.16059	7.63E-11	-4.4902	Mm.56404.1	outer dense fiber	spermatids
1457659_PM_x_at	**Odf1**	162.8154	1.27E-18	-4.6916	Mm.87367.1	outer dense fiber	spermatids
1455541_PM_a_at	**4430402I18Rik**	1.58E-13	7.60E-12	-4.7344	Mm.220899.2	SPATA6L; myosin light chain binding	connecting piece of sperm
1429471_PM_at	**1110017D15Rik**	6.41E-15	5.22E-13	-4.7819	Mm.45614.1	SMRP1; manchette	elongating spermatids
1429864_PM_at	**Spatc1**	3.05E-19	2.59E-16	-4.9207	Mm.159156.1	centriole	neck region of sperm
1440821_PM_x_at	**Odf1**	286.7803	1.06E-21	-5.0527	Mm.72475.1	outer dense fiber	spermatids
1430351_PM_at	**Spata18**	1.19E-15	1.34E-13	-5.0771	Mm.87067.1	Mitochondria-eating protein in midpiece	elongating spermatids
1418303_PM_at	**H2afb1**	4.67E-17	1.09E-14	-5.627	Mm.23887.1	replaces conventional H2A in condensation	spermatids
1431384_PM_at	**Spem1**	4.35E-17	1.05E-14	-5.7079	Mm.159159.1	manchette, cytoplasm removal	elongating spermatids
1418956_PM_at	**Tssk6**	1.89E-18	8.15E-16	-6.1185	Mm.69431.1	postmeiotic DNA condensation	ejaculated sperm

 doi:10.20944/preprints202204.0245.v1

Table S3. Mass-spectrometry data. Data of proteome measurements by MS contains UniProt accession number, gene symbol, and normalized abundances for each sample. Log2 rations, p-values from two-sided, unpaired t-tests and fold changes were calculated for each group comparison. Data were compiled for the three age groups P17, P21, and P27.